Title
ONE-BODY DISSIPATION AND THE SUPER-VISCIDITY OF NUCLEI

Author
Blocki, J.

Publication Date
1977-08-01

Submitted to Annals of Physics

Preprint

ONE-BODY DISSIPATION AND THE SUPER-VISCIDITY OF NUCLEI

J. Blocki, Y. Boneh, J. R. Nix,
J. Randrup, M. Robel, A. J. Sierk, and W. J. Swiatecki

August 10, 1977

Prepared for the U. S. Energy Research and
Development Administration under Contract W-7405-ENG-48

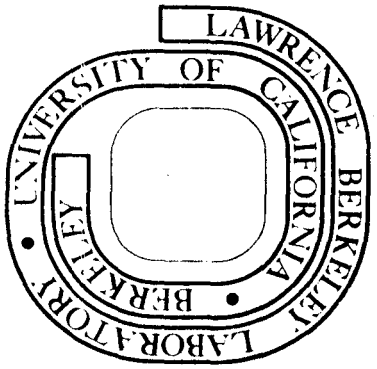

DISCLAIMER

ONE-BODY DISSIPATION AND THE SUPER-VISCIDITY OF NUCLEI*

J. Blocki,** Y. Boneh,*** J. R. Nix,† J. Randrup,†† M. Robel, A. J. Sierk,††† and W. J. Swiatecki

Nuclear Science Division
Lawrence Berkeley Laboratory
University of California
Berkeley, California 94720

August 10, 1977

ABSTRACT

This is a study of a type of fluid dynamics dominated by a "one-body" dissipation mechanism expected to be relevant for an assembly of particles whose mean free paths are comparable to or larger than the size of the system. Two simple dissipation formulae are derived, one relevant for the process of nuclear fission and the other for nuclear collisions. The resulting predictions, free of adjustable parameters, are compared quantitatively with measured fission-fragment kinetic

---

*This work was done with partial support from the U. S. Energy Research and Development Administration.

**Permanent address: Institute for Nuclear Research, Swierk, Poland.

***Permanent address: Weizmann Institute, Rehovot, Israel.

†Los Alamos Scientific Laboratory, Los Alamos, NM.

††Permanent address: Niels Bohr Institute, Copenhagen, Denmark.

†††Los Alamos Scientific Laboratory, Los Alamos, NM, and California Institute of Technology, Pasadena, CA.

energies and qualitatively with nucleus-nucleus collision data. The one-body dissipation concept is also tested against classical and quantal computer studies of particles in a deforming potential well. This brings out special effects associated with the symmetries of the well and points to a macroscopic dynamics of nuclear deformations which, except for super-fluidity at very low temperatures, consists of a smooth background dominated by one-body dissipation ("super-viscidity" of nuclei), on which are superposed modifications due to symmetries and quantization.

1. INTRODUCTION

Equations of motion, including those governing the flow of many familiar fluids, usually consist of three terms, which represent the balance between conservative, dissipative and inertial forces. The dissipative effects in fluid dynamics are often bulk phenomena arising from the viscous shearing stresses between adjacent layers of fluid in nonuniform motion. The rate of energy dissipation, i.e. the rate of flow of energy from collective degrees of freedom into microscopic (molecular) degrees of freedom, may then be expressed as a volume integral (over the bulk of the fluid) of a suitable function of the derivatives of the fluid velocity components at each point. (An explicit formula of this type is displayed in Section 4, eq. (4.1).) The microscopic mechanism for the above energy dissipation has its roots in the (two-body) interactions between the molecules of the fluid, and the physical content and mathematical structure of conventional fluid dynamics is governed by the shortness of the resulting mean-free-paths of the molecules compared to the size of the system.

This "two-body/short-path" dissipation mechanism may be contrasted with a different, "one-body/long-path" mechanism, in which the exchange of energy between collective and microscopic degrees of freedom proceeds through collisions of the particles with a moving boundary of the system. This mechanism would operate even if there were no forces between the particles, as in the case of an ideal gas of noninteracting mass points bouncing about in a deforming container. In this case the rate of energy exchange between

the mass points and the moving walls, calculated (see below) to the first order in the ratio of wall to particle velocities, leads to the ideal gas law stating the proportionality between the product of pressure and volume, and the temperature. The temperature is itself proportional to the total kinetic energy K. E. of the molecules, so that

$$pV = NRT = \frac{2}{3}\,(\text{K.E.}) \quad , \tag{1.1}$$

where N is the number of molecules and R is the gas constant (p. 116, ref 1). Thus in a slow compression of an ideal gas by a piston the collective energy of the piston is converted into the microscopic kinetic energy of the molecules. Since this result follows from a calculation to first order in the wall velocity the resulting energy expression is odd in this velocity and hence the energy flow has to be reversible: on retracting the piston slowly all of the microscopic energy reappears as macroscopic work done on the piston. The underlying mechanism of this familiar energy flow in the case of an ideal gas is just the exchange of energy between a particle and a moving wall, more specifically the increase or decrease in the speed of a particle bouncing off an approaching or receding wall.

By calculating the energy flow between wall and particles to the next order in the ratio of wall to particle speeds one expects to find a term quadratic in the wall velocities, which would then represent an <u>irreversible</u> dissipative flow of energy from the collective degrees of freedom. An example of such a calculation results, under certain assumptions, in the following simple expression

for the rate of flow of energy $\dot{E}$ into a gas with mass density ρ, composed of independent particles with average speed $\bar{v}$, and contained in a vessel of fixed volume, whose walls deform with normal velocities $\dot{n}$:

$$\dot{E} = \rho\bar{v}\oint \dot{n}^2 \, d\sigma \quad . \tag{1.2}$$

(The integral is over the surface of the vessel and the bulk of the gas is assumed to be at rest — for a derivation see Section 2. The case when the bulk of the gas is not at rest is discussed in Section 7.)

The one-body/long-path type of dissipation, exemplified by eq. (1.2) has, naturally enough, received in the past less attention than the standard two-body dissipation which is dominant for many ordinary liquids and gases. (But see refs. 2.) Nevertheless one would expect that the one-body dissipation might be relevant for a rarefied (Knudsen) gas (ref. 3) with a mean free path comparable to or longer than the dimensions of a vessel deforming at a rate no longer negligible in comparison with molecular speeds. Also for small systems at temperatures close to the absolute zero, such as nuclei or liquid He^3, for which the particle mean free path may again become comparable to the dimensions of the system, the one-body dissipation mechanism would be expected to become important. (See especially ref. 4.)

In the present paper we shall describe a tentative study of the one-body dissipation mechanism and of the possible consequences for the dynamics of nuclear systems. In Section 2 we shall derive the dissipation formula (1.2) (the "wall formula") as well as a related dissipation expression (the "window formula") relevant for

the case of two vessels (e.g. idealized nuclei in a grazing collision) exchanging noninteracting particles through a small opening or window. We shall also illustrate the generally large damping predicted, in the nuclear context, by the one-body dissipation mechanism. In Section 3 we shall explore this further by adding the wall formula expression to the usual equations of motion for the small deformations of an idealized charged nuclear drop. In Section 4 we shall describe a calculation in which the above idealized nuclear drop with damping is followed through the fission process, and we shall compare the resulting kinetic energies of the fission fragments with experiment. In Section 5 we shall attempt an estimate of the relation of the window formula to experiments on grazing and deep-inelastic collisions between nuclei. Section 6 is concerned with clarifying the foundations of the wall formula and testing it against classical and quantal computer studies of particles moving inside a deforming vessel.

In Section 7 we shall generalize the wall formula to include translations and rotation of the vessel containing the gas and then we shall discuss the formal structure of the new dynamics which follows when the motion of a fluid is dominated by the one-body dissipation mechanism. Section 8 summarizes the paper.

2. DERIVATION OF TWO DISSIPATION FORMULAE

2.1 The Wall Formula

Consider first the evaluation of the pressure acting on an element of area $\Delta\sigma$ of a plane container wall or piston in the case when the wall begins, at time $t = 0$, to move with a constant normal velocity $\dot{q}$ relative to a large volume of an ideal gas of uniform mass

density ρ , consisting of mass points m whose velocities are originally isotropic and specified by a velocity distribution function f .

Choose a coordinate system moving with the element of area $\Delta\sigma$, with the z-axis along the normal to $\Delta\sigma$ (and pointing away from the gas), and the x and y axes in the plane of $\Delta\sigma$. Let the velocity of the gas as seen from this reference frame be $\vec{U}$, so that $\dot{q}$ is the negative of the z-component, U_z , of $\vec{U}$. (To anticipate the discussion in Section 7, the velocity $\vec{U}$ characterizes the drift, with respect to the surface $\Delta\sigma$, of particles about to strike this surface. Particles not about to strike the element $\Delta\sigma$, i.e. those whose velocities are directed away from it might, in general, be characterized by a different drift velocity.)

In the reference frame moving with $\Delta\sigma$ the velocities $\vec{v}$ of the particles of the gas are clustered in velocity space around a point specified by $\vec{U}$, the density fall-off of the isotropic cluster being described by the function f (a Gaussian for a Maxwell-Boltzmann gas, a step function for a completely degenerate Fermi gas). See Fig. 1.

We shall presently require the projected velocity distribution function $g(v_z)$ which, when multiplied by dv_z, gives the fraction of particles with velocities between v_z and $v_z + dv_z$. It is obtained by integrating over particles in a slab between v_z and $v_z + dv_z$ in Fig. 1, and the result is readily found to be

$$g(v_z) = \int_{v=v_z-U_z}^{\infty} dv \; 2\pi v \, f(v) \quad . \tag{2.1}$$

For v_z less than U_z, when the lower limit is negative, the value of the function f is to be taken as the symmetric continuation to negative arguments according to $f(-v) = f(v)$. We also note the result, to be used presently, that the derivative of $g(v_z)$ is given by

$$g'(v_z) = -2\pi(v_z - U_z)\, f(v_z - U_z). \tag{2.2}$$

At a time Δt after the beginning of the motion of the wall with respect to the gas, a particle initially in a slab of width $d\ell$ parallel to the wall and at a distance ℓ from the original wall position, will have collided with the wall if its velocity v_z in the direction of the wall is such that $v_z\, \Delta t > \ell$. Each colliding particle imparts to the wall a normal momentum of magnitude $2mv_z$. The number of particles per unit area of the slab $d\ell$ is $(\rho/m)\, d\ell$, and of these a fraction $g(v_z)\, dv_z$ has a z-component of velocity between v_z and $v_z + dv_z$. The pressure on the wall, which is the momentum imparted per unit area per unit time, is therefore given by

$$p = \frac{1}{\Delta t} \iint 2m\, v_z \cdot (\rho/m)\, d\ell \cdot g(v_z)\, dv_z \quad , \tag{2.3}$$

where the region of integration over ℓ and v_z is defined by the inequality $0 < \ell < v_z \Delta t$ (see Fig. 2). Since the integrand is independent of ℓ we find at once

$$p = 2\rho \int dv_z\, v_z^2\, g(v_z) \quad . \tag{2.4}$$

Integrating by parts, using eq. (2.2), and assuming that $g(v_z)$ falls off sufficiently rapidly so that $\frac{1}{3} v_z^3 \; g(v_z)$ vanishes at infinity, we find

$$p = \rho \int_0^\infty \frac{1}{3} v_z^3 \; 4\pi (v_z - U_z) f(v_z - U_z) \, dv_z , \tag{2.5}$$

Changing the variable of integration to v, defined as $v_z - U_z$ (or $v_z + \dot{q}$), we find

$$p = \rho \int_0^\infty \frac{1}{3}(v + U_z)^3 \; 4\pi v f(v) \, dv_z - \rho \int_0^{-U_z} \frac{1}{3}(v + U_z)^3 \; 4\pi v \; f(v) \, dv_z$$

$$= \rho \, \overline{\frac{1}{3}(v - \dot{q})^3 / v} + \Delta p$$

$$= \frac{1}{3} \rho \, \overline{v^2} - \rho \bar{v} \dot{q} + \rho \dot{q} - \frac{1}{3} \rho \, \overline{v^{-1}} \, \dot{q}^3 + \Delta p \; , \tag{2.6}$$

where

$$\Delta p \equiv - \rho \int_0^{\dot{q}} \frac{1}{3}(v - \dot{q})^3 \; 4\pi v \; f(v) \, dv ,$$

and a bar denotes averaging with respect to the distribution function f(v), i.e.

$$\overline{v^n} = \int_0^\infty dv \; 4\pi \; v^2 \; f(v) \; v^n \Big/ \int_0^\infty dv \; 4\pi \; v^2 \; f(v) \quad .$$

In the case of a Fermi distribution, when f(v) is a step function dropping from $f_o = 3/(4\pi v_F^3)$ to zero at a Fermi velocity $v = v_F$, we have

$$\overline{v^n} = \frac{3}{n+3} v_F^n \quad ,$$

so that, for example, $\bar{v} = \frac{3}{4} v_F$.

The term Δp in eq. (2.6) is, for small $\dot{q}$, a very small correction of order $\dot{q}^5$. For example, in the case of the Fermi distribution mentioned above, Δp is readily calculated to be $\rho\dot{q}^5/(20v_F^3)$, if $\dot{q}$ is less than v_F.

Imagine now that instead of a plane wall moving with respect to a large body of gas we have a finite vessel whose surface elements move with normal velocities $\dot{q}$ with respect to the bulk of the gas. (The gas itself may, in general, be endowed with some drift velocity.) Insofar as the use of eq.(2.6) is justified in this case (see below), the leading term, after multiplication by the volume V of the vessel, would give

$$pV = \frac{1}{3} V \rho\overline{v^2} = \frac{2}{3} (KE),$$

where $KE = \frac{1}{2} \rho V \overline{v^2}$ is the total kinetic energy of the molecules of the gas. This is the ideal gas law.

More generally, the energy δE fed into the gas by normal displacements δn of the surface (and appearing as an increase $\delta(KE)$ of the kinetic energy of the molecules) would be

$$\begin{aligned} \delta E &= -\oint p\, \delta n\, d\sigma \\ &= -\frac{1}{3}\rho\overline{v^2} \oint \delta n\, d\sigma + \rho\bar{v} \oint \dot{q}\, \delta n\, d\sigma + \text{terms of higher order in } \dot{q}/v \end{aligned} \qquad (2.7)$$

The leading term in eq. (2.7) would, by itself, give

$$\delta(KE) = -\frac{2}{3} (KE) \frac{\delta V}{V} ,$$

or,

$$\frac{KE}{KE_0} = \left(\frac{V}{V_0}\right)^{-\frac{2}{3}} = \left(\frac{\rho}{\rho_0}\right)^{\frac{2}{3}} \quad , \tag{2.8}$$

where the subscripts zero denote some reference values of the quantities in question. The above equation states correctly the proportionality of the kinetic energy residing in the mass points of an ideal gas to the two-thirds power of the density. (Note that this relation is exactly the same for a classical and a quantized gas - a consequence of the adiabatic invariance of the action integral, refs. 5.)

For a volume-preserving deformation the first term in eq. (2.7) vanishes. The energy change δE can now be written

$$\delta E = \rho\bar{v} \oint \dot{q}\, \delta n\, d\sigma + \ldots \tag{2.9}$$

or

$$\frac{dE}{dt} = \bar{\rho v} \oint \dot{q}\dot{n}\, d\sigma + \ldots \quad . \tag{2.10}$$

If the bulk of the gas is at rest $\dot{q}$ and $\dot{n}$ are equal and we have

$$\frac{dE}{dt} = \rho\bar{v} \oint \dot{n}^2\, d\sigma + \ldots \quad . \tag{2.11}$$

Here then is a simple expression suggesting a new form of dissipative force to be inserted into the equations of motion in certain idealized problems in fluid dynamics: the dissipative force in eq. (2.9) resisting the motion of a surface element $d\sigma$ is proportional to the normal velocity $\dot{q}$ of the surface element with

respect to the bulk of the gas. The rate of energy dissipation in eq. (2.11) is proportional to the surface integral of the square of the normal surface velocity (rather than to a volume integral over the squares of velocity gradients in the fluid, as in conventional hydrodynamics).

The central assumption involved in applying the pressure expression (2.6) (derived for the initial motion of a plane wall with respect to an infinite reservoir of randomly moving gas particles) to the individual surface elements of a finite container deforming for finite time intervals, is that each element of surface continues to be bombarded by particles as if these originated in a randomized distribution. This brings out a key hypothesis of the present treatment of dissipation, namely the hypothesis of the continued randomization of the particle motions. If the particles are assumed to be strictly independent the randomization has to rely on the collisions of the particles with the vessel boundary. If this boundary and its motion are sufficiently irregular we may expect the hypothesis to be satisfied, but if they are regular and symmetric we expect the hypothesis and the associated dissipation formulae to fail. (Weak residual interactions between the particles might help to preserve some measure of validity of the formulae, but strong interactions would, of course, invalidate the whole basis of the one-body approach to the problem of dissipation.) We shall see examples of the failure of the randomization hypothesis in Section 6. A more complete study of the effect of symmetries on the one-body dissipation is presented in ref. 6.

2.2 The Window Formula

Consider now the one-body dissipative drag between two systems, A and B, in relative motion and communicating through a small window of area $\Delta\sigma$. (Fig. 3.) As before let the velocity of a particle with respect to the window be $\vec{v}$ and the velocity of the gas with respect to the window be $\vec{U}$ for A and $\vec{U}'$ for B. (The velocities $\vec{U},\vec{U}'$ again characterize the drift velocities, with respect to the window, of particles about to traverse it.) Let the velocity of the window with respect to an inertial system of coordinates be $\vec{W}$, so that with respect to this system the particle and drift velocities are $\vec{v} + \vec{W}$, $\vec{U} + \vec{W}$ and $\vec{U}' + \vec{W}$.

The window $\Delta\sigma$ may be considered to divide the total system of particles into two sub-systems, one consisting of the particles which at any instant are in part A and one consisting of the particles in part B. The force $\vec{F}_A$ on sub-system A is equal to the rate of change of momentum of this group of particles and consists of three parts: (1) the rate of change of momentum due to the collisions of the particles with the open surface, denoted by $A - \Delta\sigma$, of container A, (2) the flux of momentum $\vec{\mathscr{P}}_{BA}$ from container B into container A, and (3) the negative of the flux of momentum $\vec{\mathscr{P}}_{AB}$ from A into B. Thus

$$\vec{F}_A = \int_{A-\Delta\sigma} (-p\check{n})\, d\sigma + \vec{\mathscr{P}}_{BA}\,\Delta\sigma - \vec{\mathscr{P}}_{AB}\,\Delta\sigma\ , \tag{2.12}$$

where p is the pressure exerted by the gas on the walls of container A, and $\check{n}$ is the outward unit vector along the direction normal to the surface.

In order to calculate the momentum flux $\vec{\mathscr{P}}_{AB}$ we shall use exactly the same considerations and the same ℓ vs v_z diagram as in

the case of the pressure calculation in Section 2.1, except that each particle, instead of contributing a momentum change $2m\, v_z$ on hitting a wall element, contributes a momentum loss from the container equal to $m(\vec{v}+\vec{W})$. We shall re-write this as $m[\vec{U} + (\vec{v}-\vec{U}) + \vec{W}]$ in order to deduce by inspection that, for particles in a slab dv_z in velocity space (see Fig. 1) the average momentum loss per particle is $m[\vec{U} + (v_z - U_z)\breve{z} + \vec{W}]$. (Here $\breve{z}$ is the unit vector along the z-axis, assumed to point in the direction of the normal to $\Delta\sigma$, from A towards B.) This is because the x and y components of $\vec{v}-\vec{U}$ (the velocity with respect to $\vec{U}$) average out to zero by symmetry (see Fig. 1). We may further re-write the above expression as $m(\vec{U}_\perp + \vec{W} + v_z\breve{z})$, where $\vec{U}_\perp$ is the two-dimensional vector component of $\vec{U}$ in the x,y plane. It now follows that in order to find $\vec{\mathscr{P}}_{AB}$ we merely replace $2m\, v_z$ in eq. (2.3) by $m(\vec{U}_\perp + \vec{W} + v_z\breve{z})$, to obtain

$$\vec{\mathscr{P}}_{AB} = \frac{1}{\Delta t}\iint m(\vec{U}_\perp+\vec{W}+v_z\breve{z})\cdot(\rho/m)d\ell\cdot g(v_z)dv_z$$

$$= \int_0^\infty dv_z(\vec{U}_\perp+\vec{W}+v_z\breve{z})\; v_z g(v_z). \qquad (2.13)$$

The second part of this integral is proportional to exactly the same integral over v_z as the one in eq. (2.4). The first part differs by having one power of v_z less. The result of integrating eq. (2.13) by parts and manipulating the expression as before is, therefore, (by inspection)

$$\vec{\mathscr{P}}_{AB} = \frac{1}{2}\rho\left\{(\vec{U}_\perp+\vec{W})\overline{\tfrac{1}{2}(v+U_z)^2/v} + \breve{z}\,\overline{\tfrac{1}{3}(v+U_z)^3/v}\right\} + \Delta\vec{\mathscr{P}}_{AB},$$

where (2.14)

$$\Delta\vec{\mathscr{P}}_{AB} = -\rho\int_0^{-U_z} dv\left[\tfrac{1}{2}(v+U_z)^2(\vec{U}_\perp+\vec{W})+\tfrac{1}{3}(v+U_z)^3\breve{z}\right]2\pi v f(v)\ .$$

For small $\vec{U}$ the term $\Delta\vec{\mathscr{P}}_{AB}$ is a very small correction of order U^5.

In order to obtain the momentum flux $\vec{\mathscr{P}}_{BA}$ from B to A we merely replace $\vec{U}_\perp$ by $\vec{U}_\perp'$, U_z by $-U_z'$ and change the sign of $\breve{z}$ in eq. (16) (since the direction of the z-axis is into container B). Thus

$$\vec{\mathscr{P}}_{BA} = \frac{1}{2}\rho\left\{(\vec{U}_\perp'+\vec{W})\overline{\frac{1}{2}(v-U_z')^2/v} - \breve{z}\,\overline{\frac{1}{3}(v-U_z')^3/v}\right\} + \Delta\vec{\mathscr{P}}_{BA} \quad , \tag{2.15}$$

$$\Delta\vec{\mathscr{P}}_{BA} = -\rho\int_0^{-U_z'} dv\left[\frac{1}{2}(v-U_z')^2\ (\vec{U}_\perp'+\vec{W}) - \frac{1}{3}(v-U_z')^3\,\breve{z}\right]\ 2\pi v f(v).$$

Substitution of eqs. (2.14), (2.15) into eq. (2.12) now gives the force on system A, without any assumptions as to the smallness of the velocities $\vec{U}$, $\vec{U}'$ and $\vec{W}$ with respect to typical particle speeds $\bar{v}$. If these velocities are small and we retain only the leading terms in these quantities we find

$$\vec{\mathscr{P}}_{AB} = \frac{1}{2}\rho\left\{\frac{1}{2}\bar{v}\,(\vec{U}_\perp+\vec{W}) + (\frac{1}{3}\overline{v^2}+\bar{v}\,U_z)\,\breve{z} + \ldots\right\} ,$$

which leads to

$$\begin{aligned}\vec{F} = &\int_{A-\Delta\sigma}(-p\breve{n})d\sigma - \frac{1}{3}\rho\overline{v^2}\,\breve{z}\Delta\sigma \\ &+ \frac{1}{2}\rho\,\Delta\sigma\left\{\breve{z}\bar{v}(U_z'-U_z) + \frac{1}{2}\bar{v}(\vec{U}_\perp'-\vec{U}_\perp) + \ldots\right\} .\end{aligned} \tag{2.16}$$

If the surface elements of container A are not in motion with respect to the gas inside it, the pressure p is given by the static

value $\frac{1}{3}\rho\overline{v^2}$. The first line in eq. (2.16) is then an integral of a constant pressure taken over a closed surface (closed off by the term in $\Delta\sigma$), and the result is identically zero. If the surface elements are in motion with respect to the gas there will be an additional contribution to the force on A, of the form of the wall formula discussed in Section 2.1, and associated with the container A itself. In any case the force on A due to the presence of B is given by the second line in eq. (2.16). We shall denote it by $\vec{F}_{B \text{ on } A}$, or $\vec{F}_{BA}$. It can be written as

$$\vec{F}_{BA} = n_o \Delta\sigma(2\vec{u}_{\parallel} + \vec{u}_{\perp}) + \ldots , \tag{2.17}$$

where $\vec{u}$, equal to $\vec{U}' - \vec{U}$, is the velocity of B relative to A, and $\vec{u}_{\parallel}$ and $\vec{u}_{\perp}$ are the components of this velocity along and at right angles to the normal through the window $\Delta\sigma$ (pointing from A to B). The quantity n_o, equal to $\frac{1}{4}\rho\bar{v}$, is the static one-sided flux of particles in the gas (from left to right or right to left across a unit area).

Equation (2.17) is the window formula for the velocity-dependent dissipative drag of system B on system A calculated to first order in the relative velocity $\vec{u}$. Note that this force is not, in general, parallel to $\vec{u}$, since the friction coefficient associated with motion normal to the window is twice the corresponding coefficient for tangential friction. The reason for this may be traced to the circumstance that the normal component of the motion (unlike the tangential component) affects the rate of exchange of particles between the two containers. Note also that to the first order in the velocities $\vec{U}, \vec{U}', \vec{W}$ the window formula (2.17)

is independent of the window velocity $\vec{W}$. Taken to higher orders the formula would contain a term linear in $\vec{W}$ associated with the mass flux between the containers.

In the nuclear context we shall use a velocity or momentum distribution which is constant up to a maximum Fermi velocity v_F or Fermi momentum $P = mv_F$, so that

$$\bar{v} = (3/4)v_F \quad . \tag{2.18}$$

With four nucleons per h^3 of phase space (h is Planck's constant) the particle density ρ/m is related to P through

$$\left(\frac{4}{3}\pi P^3\right) \; 4/h^3 \; = \rho/m \; = \left(\frac{4}{3}\pi r_0{}^3 \, m\right)^{-1} \tag{2.19}$$

where m is the nucleon mass and r_0 the nuclear radius constant. Using these relations the quantity $\rho\bar{v}$ appearing in the wall formula eq. (2) can be written as $4\pi P^4/h^3$, and the drag coefficient $\frac{1}{4}\rho\bar{v}$ in the window formula eq. (2.17) is simply $\pi P^4/h^3$. For tangential motion, when $u_{\|} = 0$, the window formula reduces to the result quoted on p. 55 in ref. 7 .

We may note here that the reservations one might have concerning our derivation of the wall and window dissipation formulae, on account of the disregard in those derivations of the Pauli exclusion principle, are largely removed by the correspondence between classical and quantum mechanics revealed by Liouville's theorem. According to this theorem the representative points in phase space, for classical particles moving under the influence of a time-dependent one-body potential, exhibit the properties of an incompressible fluid. It follows that if a swarm

of particles is distributed so as to satisfy the exclusion principle initially (by having, say, four particles per h^3 of phase space) the classical equations of motion ensure that the principle will be obeyed for all time, at least in the average sense of a fixed density $4/h^3$ in phase space.

2.3 Characteristic Damping Times for Nuclei

We note that there is nothing adjustable in the wall and window formulae. When applied to the nuclear situation, the nuclear density ρ is known and the mean nucleonic speed $\bar{v}$ is known. Thus we can at once make an estimate to see whether the dynamics of a nucleus described by the independent-particle (Knudsen-gas) model should be dominated by dissipation or not. The simple order-of-magnitude way of doing this is to write down the characteristic decay or damping time of the one-body dissipation theory resulting from balancing typical inertial and dissipative terms in the equations of motion. For example, if in the fission process we imagine a nucleus (radius R), started off with a collective kinetic energy E (in the form of a surface deformation or ripple of multiple order ℓ, say) the time to dissipate this collective energy will be of the order of

$$t_{damp} \approx \left| \frac{1}{E} \frac{dE}{dt} \right|^{-1} .$$

Let us write the wall-formula estimate for dE/dt as

$$\left| \frac{dE}{dt} \right| \approx \rho\bar{v}(4\pi R^2)(\text{typical } \dot{n}^2) \quad ,$$

and the estimate for the kinetic energy E as one half a typical mass times a typical value of $\dot{n}^2$. The typical mass in a multipole ripple of order ℓ is of the order of $\frac{1}{\ell}$ (mass of nucleus), because the nodes of the multipole ripple divide the nucleus into about ℓ cells. Dropping all numerical factors we then find the order of magnitude relation

$$t_{damping} \approx \frac{1}{\ell} \quad (R/\bar{v})$$

$\frac{1}{\ell}$: Geometrical factor

$(R/\bar{v})$: Characteristic time unit of the one-body dissipation theory.

The characteristic time unit is thus a nucleon transit time. It is in the range of $(0.7 - 1.3) \times 10^{-22}$ sec for mass numbers between 50 and 250. (The corresponding damping widths in energy units would be $\hbar(\bar{v}/R) \approx$ 5 - 9 MeV.) These are damping times intrinsically short compared to many characteristic collective times, so the message here is that one-body energy dissipation may often dominate collective nuclear dynamics. The mechanism of collective energy dissipation by collisions of particles with the moving walls of the potential well appears to be not some small correction, but a gross, dominating phenomenon that has to be

looked at very seriously. It suggests at once that nuclei may often be "super-viscid".

A similar order-of-magnitude estimate of the damping or stopping time in nucleus-nucleus collisions goes as follows. Imagine two nuclei with radii R colliding with a relative velocity u. The collective kinetic energy is of order

$$E \approx \left(\frac{4}{3}\pi R^3 \rho\right) u^2.$$

(We are again dropping factors of order one.) If the nuclei are in communication through a neck or window of area πa^2 the window formula says

$$\left|\frac{dE}{dt}\right| \approx \frac{1}{4}\rho\bar{v}(\pi a^2)(u^2).$$

Therefore the characteristic damping or stopping time is of order

$$t_{stop} \approx R^3\rho u^2/\rho\bar{v}a^2u^2 \approx (R/a)^2(R/\bar{v})$$

(Geometrical factor; Characteristic time unit.)

Again we see the product of a geometrical factor and the characteristic (short) nucleonic time unit. If we compare this stopping time with a collision time defined by

$$t_{coll} \approx \frac{R}{u}$$

we find

$$\frac{t_{stop}}{t_{coll}} \approx (R/a)^2(u/\bar{v}),$$

or

$$\frac{t_{stop}}{t_{coll}} \approx (R/a)^2 \sqrt{\frac{\text{Energy per nucleon above barrier}}{\text{Fermi energy } (\sim 30 \text{ MeV})}} \quad .$$

Here the geometrical factor $(R/a)^2$ is all-important — the stopping time goes of course to ∞ as the neck a tends to zero. But for not too small necks the above ratio might be of order 1 if the total energy above the barrier is not too many MeV. In that case the super-viscid nuclei might be brought to relative rest in a time comparable to the collision time, as required by the phenomenon of deep inelastic scattering.

This is the background of the idea of one-body dissipation and of nuclear super-viscidity. How does the idea fare when subjected to further theoretical analysis and confronted with experiment? In order to answer this question and to learn under what conditions — if ever — simple expressions of the type of eqs. (2.11) and (2.17) are relevant for practical applications, we shall proceed in two ways. In Section 6 we shall attempt a discussion of the validity of the assumptions underlying these equations. Subtle questions are involved to some of which we don't know the answer. Even pending the further clarification of these questions we have thought it worthwhile to explore, in Sections 3, 4, and 5, some consequences of these equations and to compare the results with experimental data on nuclear dynamics, especially nuclear fission.

3. SMALL VIBRATIONS OF A DROP

The order of magnitude of the dissipation associated with eq. (2.11) in the context of nuclear dynamics may be illustrated by adding such a term to the equations of motion of an idealized incompressible nuclear drop (with a surface tension γ and a uniformly distributed total charge Ze) that is undergoing small motion around the spherical shape.

Let the radius vector of the surface be written as

$$R(\theta,\phi) = \frac{R_0}{\lambda}\left[1 + \sum_{\ell=1}^{\infty}\sum_{m=-\ell}^{\ell} a_{\ell m}\, Y_{\ell m}(\theta,\phi)\right] , \qquad (3.1)$$

with $a^*_{\ell m} = (-1)^m a_{\ell,-m}$ (to ensure the reality of R), λ a scale factor ensuring conservation of volume, and the terms with $\ell = 1$ ensuring the fixity of the center of mass. In what follows we shall restrict ourselves to the case of <u>real</u> coefficients $a_{\ell m}$. This corresponds to standing waves which carry no angular momentum.

The changes in the surface and Coulomb energies of the distorted drop are given by (ref. 8)

$$\Delta E_s = \frac{1}{2} R_0^2 \gamma \sum_{2}^{\infty}\sum_{-\ell}^{\ell} (\ell-1)(\ell+2)\, a_{\ell m}^2 + \ldots ,$$

$$\Delta E_c = -\frac{3}{4\pi}\frac{(Ze)^2}{R_0}\sum_{2}^{\infty}\sum_{-\ell}^{\ell}\frac{(\ell-1)}{(2\ell+1)}\, a_{\ell m}^2 + \ldots ,$$

so that the potential energy of the drop with respect to the spherical shape may be written as

$$V = \frac{1}{2} \sum_{2}^{\infty} \sum_{-\ell}^{\ell} C_\ell \, a_{\ell m}{}^2 + \ldots \quad , \tag{3.2}$$

where

$$C_\ell = R_0{}^2 \gamma \left[(\ell - 1)(\ell + 2) - \frac{20x(\ell - 1)}{2\ell + 1} \right] \quad , \tag{3.3}$$

and x is the fissility parameter defined by $(Ze)^2/[10(\frac{4}{3}\pi R_0{}^3)\gamma]$.

If, for purposes of illustration, we assume irrotational flow, the kinetic energy is (ref. 8)

$$KE = \frac{1}{2} \sum_{2}^{\infty} \sum_{-\ell}^{\ell} M_\ell a_{\ell m}{}^2 + \ldots \quad , \tag{3.4}$$

where $M_\ell = \rho R_0{}^5/\ell$.

It follows that the force resisting an increase $da_{\ell m}$ in one of the coefficients $a_{\ell m}$ is $-\frac{\partial V}{\partial a_{\ell m}} = -C_\ell \, a_{\ell m}$, and that the inertial reaction associated with an acceleration $\ddot{a}_{\ell m}$ in $a_{\ell m}$ is $-M_\ell \ddot{a}_{\ell m}$.

The dissipative force may be deduced with the aid of eq. (2.11). Using

$$\dot{n} = R_0 \sum_{2}^{\infty} \sum_{-\ell}^{\ell} \dot{a}_{\ell m} Y_{\ell m} + \ldots \quad ,$$

$$\delta n = R_0 \sum_{2}^{\infty} \sum_{-\ell}^{\ell} \delta a_{\ell m} Y_{\ell m} + \ldots$$

$$= R_0 \sum_{2}^{\infty} \sum_{-\ell}^{\ell} \delta a_{\ell m} Y^*_{\ell m} + \ldots \quad ,$$

we find for the energy dissipated in a displacement δn the result

$$\delta E = \rho\bar{v}R_0^2 \oint \left(\sum\sum \dot{a}_{\ell m} Y_{\ell m}\right)\left(\sum\sum \delta a_{\ell m} Y^*_{\ell m} + \ldots\right)$$

$$= R_0^4 \rho\bar{v} \sum_{2}^{\infty} \sum_{-\ell}^{\ell} \dot{a}_{\ell m}\delta a_{\ell m} + \ldots \quad .$$

It follows that the dissipative force associated with a rate of change $\dot{a}_{\ell m}$ in $a_{\ell m}$ is given by $-D\dot{a}_{\ell m}$, where $D = R_0^4\rho\bar{v}$. (Note that this friction term is independent of ℓ.)

The balance of inertial, dissipative and conservative forces requires that

$$M_\ell \ddot{a}_{\ell m} + D\,\dot{a}_{\ell m} + C_\ell a_{\ell m} = 0 \quad . \tag{3.5}$$

We note that if the damping were due to ordinary (two-body) viscosity the equations of motion (again under the illustrative assumption of irrotational flow) would be

$$M_\ell \ddot{a}_{\ell m} + D_\ell \dot{a}_{\ell m} + C_\ell a_{\ell m} = 0 \quad , \tag{3.6}$$

where[9,10]

$$D_\ell = 2\mu R_0^3 \,(\ell-1)(2\ell+1)/\ell \quad ,$$

μ being the usual viscosity coefficient of the fluid.

In the absence of dissipation the characteristic time of the collective vibrations described by eq. (3.5) or (3.6) would be

$$T_{vib} = \sqrt{\frac{M_\ell}{C_\ell}} \quad .$$

On the other hand in the absence of driving forces (i.e. $C_\ell = 0$) the e-folding time for the damping of an initial motion would be given by

$$t_{damp}^{(1)} = \frac{M_\ell}{D} = \frac{R_0^5 \rho/\ell}{R_0^4 \rho \bar{v}} = \frac{1}{\ell} (R_0/\bar{v}) \tag{3.7a}$$

in the case of one-body dissipation, and

$$t_{damp}^{(2)} = \frac{M_\ell}{D_\ell} = \frac{1}{2(\ell-1)(2\ell+1)} (R_0^2 \rho/\mu) \tag{3.7b}$$

in the case of two-body dissipation.

Equation (3.7) re-states quantitatively the order-of-magnitude result found in Section 2.3 , according to which the fundamental time unit of the one-body dissipation dynamics is the transit time $R_0/\bar{v}$. Similarly the fundamental time unit for dynamics dominated by two-body dissipation is given by the expression $R_0^2 \rho/\mu$ in eq. (3.7a), which may be rewritten in an instructive way by using an estimate for the viscosity coefficient which follows from the kinetic theory of gases, viz

$$\mu = \frac{1}{3} \rho \bar{v} L \quad , \tag{3.8}$$

where L is a suitable mean free path of the particles in the gas (see p. 273, ref.1). This leads to

$$t_{damp}^{(2)} = \frac{3}{2(\ell-1)(2\ell+1)} (R_0/\bar{v})(R_0/L). \tag{3.9}$$

The fundamental time unit multiplying the geometrical factor $3/2(\ell-1)(2\ell+1)$ is the transit time $(R_0/\bar{v})$ augmented by the ratio of R_0 to L. (In this case $R_0/\bar{v}$ is what the single-particle transit

time would be if there were no collisions between particles.) For macroscopic bodies R_0/L is a large factor and viscous effects for large fluid systems are thus often of secondary importance. On the other hand for small systems the damping time $t^{(2)}$ may become as short as the transit time $R_0/\sqrt{v}$, which is itself short compared to typical collective times. One would then expect such small systems to be dominated by viscosity. (This is in accordance with the observation that the dynamics of all ordinary fluids, including the Fermi liquid He^3, would be dominated by viscosity once the scale of the relevant objects reached the level where only tens or hundreds of molecules were involved - see pp. 53, 54, ref. 7.)

In the nuclear context eq. (3.9) might be relevant at very high temperatures, approaching or even exceeding the Fermi energy. (An extreme case is the recently discussed nuclear "fireball", ref. 11). At such temperatures the exclusion principle is relatively less important in inhibiting nucleon-nucleon interactions and nuclear matter is expected to become more nearly like an ordinary fluid, characterized by mean free paths of a couple of fermis. Since relevant nuclear radii are unlikely to be more than a few fermis, ratios R_0/L of around 3 may be typical and for such systems severely overdamped dynamics, with damping times of the order of the transit time $R_0/\sqrt{v}$, may again be anticipated.

Coming back to eq. (3.5) we see that each amplitude $a_{\ell m}$ obeys the equation of motion of a damped harmonic oscillator. The motion is periodic (with damped amplitude) if $D < 2\sqrt{M_\ell C_\ell}$ and aperiodic if $D > 2\sqrt{M_\ell C_\ell}$. The critical value of D is thus

$$D_{crit} = 2\sqrt{M_\ell C_\ell} = 2\sqrt{\rho R_0^7 \gamma \frac{\ell-1}{\ell}\left[\ell+2-\frac{20x}{2\ell+1}\right]} \quad . \tag{3.10}$$

A dimensionless coefficient of overdamping $\chi_\ell^{(1)}$ may be defined for each mode by

$$\chi_\ell^{(1)} \equiv \frac{D}{D_{crit}} = \frac{1}{2}\bar{v}\sqrt{\frac{R_0\rho}{\gamma}}\left[\frac{\ell-1}{\ell}\left(\ell+2-\frac{20x}{2\ell+1}\right)\right]^{-\frac{1}{2}}$$

$$\approx \frac{1}{2}\bar{v}\sqrt{\frac{\rho}{\gamma}}\left(\frac{R_0}{\ell}\right)^{\frac{1}{2}} \quad \text{for large } \ell \quad . \tag{3.11}$$

This number gives the relative importance, for a given mode, of the damping force compared to the inertial force.

Using again eqs. (2.18) and (2.19) we find for $\chi_\ell^{(1)}$ the expression

$$\chi_\ell^{(1)} = (3/16)(9\pi)^{1/3}\sqrt{3}\sqrt{(\hbar^2/mr_0)/(4\pi r_0^2)}\left[\frac{\ell-1}{\ell}\left(\ell+2-\frac{20x}{2\ell+1}\right)\right]^{-\frac{1}{2}} .$$

(In ref. 12 this formula was incorrectly written with a factor 3/8 instead of 3/16.) We give below a corrected table of the values of $\chi_\ell^{(1)}$ for three idealized nuclei and three harmonics (Lysekil parameters were used, ref. 13.)

TABLE I

	$\ell = 2$	4	8
$^{20}_{10}Ne$	1.51	0.97	0.69
$^{120}_{50}Sn$	2.62	1.44	0.97
$^{238}_{92}U$	4.73	1.79	1.14

The values of $\chi_\ell^{(1)}$ are larger than one except for very light nuclei and/or high harmonics, suggesting severely overdamped aperiodic motions in most cases. Formally this overdamping would (for a given mode) increase without limit for very large systems (see eq. (3.11)). The idealized nuclei would become "super-viscid." Table I suggests that many nuclei in the periodic table, especially the heavier ones, might exhibit to a noticeable extent such super-viscid characteristics.

A high nuclear viscosity or dissipation is indeed implied by the existence of so-called deep inelastic processes (ref. 14), which suggests that nuclei behave somewhat like two drops of honey that get stuck but do not easily flow together. However, high <u>two</u>-body viscosity is inadmissible in fission, where it would predict stretched-out scission shapes resulting in fission-fragment energies far below those observed experimentally (see ref. 15 and section 4). This stretching out is due to the stronger damping of short wavelength modes, such as a necking-in of the fissioning shape, compared to an overall elongation — exactly the mechanism that is responsible for the formation of a long neck in dripping honey. This is a well-known effect in hydrodynamics where (ordinary) viscosity always becomes dominant for sufficiently short wavelength modes (or sufficiently small systems - see above). A quantitative illustration of this is provided by eq. (3.6). This time the friction terms D_ℓ depend on ℓ (they increase linearly with ℓ for large ℓ) and the coefficient of overdamping $\chi^{(2)}$, defined in analogy with $\chi^{(1)}$, is given by

$$\chi_\ell^{(2)} \equiv \frac{D_\ell}{D_{int}} = \frac{D_\ell}{2\sqrt{M_\ell C_\ell}} = \mu(2\ell+1)\left[\rho\, R_0\, \gamma\, \frac{\ell}{\ell-1}\,(\ell+2-\frac{20x}{2\ell+1}\right]^{-\frac{1}{2}} \tag{3.12}$$

$$\approx \frac{2\mu}{\sqrt{\rho\gamma}}\left(\frac{\ell}{R_0}\right)^{1/2} \quad \text{for large } \ell \quad .$$

We readily find that the ratio of the overdamping factors for two- and one-body dissipation is

$$\frac{\chi_\ell^{(2)}}{\chi_\ell^{(1)}} = \frac{2}{3}\,(2\ell+1)(L/R_0) \quad .$$

It follows that for a mean free path of the order of 2 fm the overdamping factors $\chi^{(2)}$ would often be even larger than $\chi^{(1)}$, ranging in fact between 2.8 and 4.7 for the cases listed in Table I. We may also note that for this choice of the mean free path, eq. (3.8) gives for the viscosity of (hot) nuclear matter the value $\mu = 0.12$ terapoise. This is a very high value (about eight times larger than the moderate viscosity used in ref. 18) and confirms that at least <u>hot</u> nuclear matter (along with all known normal liquids) would exhibit super-viscid characteristics when the relevant systems are sufficiently small.

Note that, since a typical harmonic of order ℓ corresponds to a ripple with a separation between nodes of order R_0/ℓ, eq. (3.12) states that the relative importance of normal viscosity is inversely proportional to the square root of the wavelength of the disturbance (for short wavelengths). In contrast, the coefficient $\chi_\ell^{(1)}$ for one-body dissipation is <u>directly</u> proportional to the square root of the wavelength

(eq. (3.11)). The reason for the extra power of a wavelength λ in the ratio $\chi^{(1)}/\chi^{(2)}$ (or in the ratio $t^{(2)}/t^{(1)}$) is immediately clear from the expressions for the rate of energy dissipation $\dot{E}$ in the two cases: a surface integral of the square of the surface velocity in the first case (eq. (2.11)), and a volume integral over the squares of velocity gradients, in the second. To see this consider a wave of wavelength λ on a plane fluid surface. Let the amplitude change at a rate $\dot{n}$. The rate of one-body energy dissipation is proportional to $(\dot{n})^2$ (area), and is independent of λ. In the case of normal hydrodynamics a wave of wavelength λ disturbs a layer of fluid to a depth of the order of λ below the surface (ref. 16). The velocity gradients are therefore of order $\dot{n}/\lambda$ and the volume of affected fluid is of order (area) (λ). Hence the volume integral over the square of the velocity gradient is proportional to (area) (λ) $(\dot{n}/\lambda)^2$ = (area) $(\dot{n})^2/\lambda$. This explains the extra power of λ and the inhibition of short wavelength modes (like necking) in hydrodynamics with ordinary viscosity. In the case of one-body damping such an inhibition of short wavelength modes is not present, and it is therefore quite possible that in a fission process dominated by one-body dissipation the scission shapes would be reasonably compact and the fission fragment kinetic energies would not come out in drastic disagreement with experiment. In the next section this question will be investigated quantitatively.

4. FISSION OF AN IDEALIZED DROP

To explore quantitatively the effect of one-body dissipation on the dynamics of fission we use an extension of the simple macroscopic approach described in refs. 17 and 18. In particular, we describe the

shape of the nucleus by means of N collective coordinates $q = q_1, \ldots, q_N$ and solve classical equations of motion to determine their time dependence.

The presence of dissipation introduces into the equations of motion an additional force that is proportional to the generalized velocities. This modifies Lagrange's equations to[19]

$$\frac{d}{dt}\left(\frac{\partial L}{\partial \dot{q}_i}\right) = \frac{\partial L}{\partial q_i} - \frac{\partial F}{\partial \dot{q}_i} \quad , \quad i = 1, \ldots, N \quad ,$$

where the Lagrangian $L = T - V$ is the difference between the collective kinetic and potential energies and where F is the Rayleigh dissipation function; $\dot{q}_i$ denotes the collective velocity corresponding to q_i. These N second-order differential equations are transformed into 2N first-order differential equations for the coordinates and their conjugate momenta (modified Hamilton's equations), which are integrated numerically to determine the time evolution of the system for a given set of initial conditions.

The dynamical motion therefore depends in general upon the nuclear potential energy of deformation $V(q)$, upon the collective kinetic energy $T(q,\dot{q})$, and upon the Rayleigh dissipation function $F(q,\dot{q})$. The nuclear potential energy is calculated by means of a modified liquid-drop model[20,21] that takes into account effects due to the finite range of the nuclear force in addition to the surface and Coulomb energies of the ordinary liquid-drop model. In this model, the nuclear macroscopic energy is determined in terms of a double volume integral of a Yukawa function. Because we neglect single-particle corrections to the potential energy,

our later comparisons with experimental data must be restricted to nuclei with moderately high excitation energies, where single-particle effects are expected to become relatively small.

The collective kinetic energy is calculated for incompressible, nearly irrotational hydrodynamical flow by use of the Werner-Wheeler method,[18,22] which approximates the true velocity field $\vec{v}$ inside the nucleus by the flow of circular layers of fluid. When the dissipation is small the dynamical motion is affected strongly by the kinetic energy. However, for large dissipation, such as the one-body dissipation considered here, the dynamical motion is relatively independent of the kinetic energy. Therefore, in this limit, the deficiencies of the Werner-Wheeler method become unimportant.

For the ordinary two-body viscosity considered in refs. 17 and 18, the Rayleigh dissipation function (equal to half the rate of energy dissipation) is calculated by means of the standard volume integral of fluid dynamics[23]

$$F = \frac{1}{2}\mu\int\{\nabla^2 v^2 + (\nabla \times \vec{v})^2 - 2\nabla\cdot[\vec{v} \times (\nabla \times \vec{v})]\}d^3r \quad , \qquad (4.1)$$

where μ is the viscosity coefficient. (It is a volume integral over squares and products of gradients of the fluid velocity components.) For the one-body dissipation considered here, we calculate F by means of the surface integral appearing in eq. (2.11)), where $F = \frac{1}{2}\frac{dE}{dt}$.

We restrict ourselves to axially symmetric nuclei and describe the shape of a fissioning nucleus prior to scission in terms of smoothly joined portions of three quadratic surfaces of revolution.[22] The results reported here are also restricted to reflection-symmetric nuclei,

which means that we consider explicitly only three deformation coordinates. These specify (1) the distance between the centers of the two end spheroids that form the shape, (2) the eccentricity of these end spheroids, and (3) the eccentricity of the middle quadratic surface that forms the neck.

For displaying the dynamical paths of fissioning nuclei it is convenient to project out of this three-dimensional space (or in general out of an infinite-dimensional space) the two most important symmetric degrees of freedom. These are defined conveniently in terms of the central moments[18,21]

$$r = 2\langle z \rangle$$

and

$$\sigma = 2\left\langle (z - \langle z \rangle)^2 \right\rangle^{1/2},$$

where the angular brackets $\langle\rangle$ denote an average over the half volume to the right of the midplane of the reflection-symmetric shape. The moment r gives the distance between the centers of mass of the two halves of the dividing nucleus, and σ gives a measure of the elongation of each half about its center of mass.

As a unit of distance it is convenient to use the radius R_0 of the spherical nucleus, which we determine according to the simple relationship

$$R_0 = r_0 A^{1/3},$$

with[18,20,21,24]

$$r_0 = 1.16 \text{ fm}.$$

In terms of the central moments r and σ we show in Fig. 4 how one-body dissipation has the opposite effect on the prescission dynamical path compared to ordinary two-body viscosity. Relative to the reference path for a nonviscous ^{236}U nucleus (dot-dashed curve), ordinary two-body viscosity shifts the dynamical path toward increased fragment elongation (dashed curves). This occurs because neck formation is a process that involves large velocity gradients and that consequently is hindered by two-body viscosity. In contrast, one-body dissipation shifts the dynamical path toward a more compact configuration (solid curve).

Strictly speaking, the initial conditions used in constructing Fig. 4 correspond to starting from the ^{236}U macroscopic saddle point with 1 MeV of kinetic energy in the fission direction for nonviscous flow. However, the most probable paths corresponding to starting from rest an infinitesimal distance from the saddle point are practically indistinguishable from those shown in Fig. 4. Furthermore, for heavy nuclei the dependence of the fission eigenvector upon dissipation is so slight that it may be safely neglected.

The opposite effects of two-body viscosity and one-body dissipation on the actual scission shapes are shown in Fig. 5 for the fission of four nuclei that span our present region of interest. As seen in the first column, for nonviscous flow the scission shapes are relatively compact for light nuclei and become more elongated for heavy nuclei. This occurs because of the increased Coulomb repulsion for heavy nuclei. The second column shows that for infinite two-body viscosity the scission shapes become more elongated, with the amount of elongation increasing for heavy nuclei. This increased elongation occurs because of the

large velocity gradients involved in neck formation, which is therefore hindered by two-body viscosity. The third column shows that for one-body dissipation the scission shapes become more compact, and that furthermore they are approximately the same for the fission of heavy nuclei as for the fission of light nuclei.

In Fig. 5 the scission shapes for ^{236}U are taken from the appropriate dyanmical paths of Fig. 4 and consequently refer strictly to starting a ^{236}U nucleus from its macroscopic saddle point with 1 MeV of initial kinetic energy in the fission direction for nonviscous flow. The scission shapes for the remaining three nuclei in Fig. 5 are calculated for nuclei along Green's approximation to the valley of β stability[25] with the indicated values of Z^2/A; the nuclei with the closest integral values of Z and A are also indicated. For these cases the scission shapes refer strictly to most probable paths. Furthermore, in calculating the most probable paths for one-body dissipation we neglect the inertia, which is an excellent approximation because the one-body dissipation tensor is so large that it dominates the solution. (The inertia is retained in calculating the ^{236}U path for one-body dissipation.) These technicalities have no visible effect on the shapes shown in Fig. 5.

We compare in Fig. 6 some results of our calculations with experimental most probable fission-fragment kinetic energies for the fission of nuclei throughout the periodic table. The experimental data all refer to moderately high excitation energies, where the most probable mass division is into two equal fragments and where single-particle effects should be relatively small. The results calculated for non-viscous flow (dot-dashed curve) agree with the experimental values for

light nuclei but are higher than the experimental values for heavy nuclei.

This discrepancy may be removed either by two-body viscosity or by one-body dissipation, but the detailed manner in which this occurs is different in the two cases. The final translational kinetic energy of the fission fragments at infinity may be decomposed conceptually into the contribution that is acquired prior to scission and the remaining contribution that is acquired from the scission point onwards. For light nuclei the relatively small distance between the saddle and scission points means that the prescission kinetic energy is always small. However, for heavy nuclei the relatively large distance between the saddle and scission points leads to a substantial prescission kinetic energy when the hydrodynamical flow is nonviscous. This prescission kinetic energy is reduced by either two-body viscosity or by one-body dissipation.

Because two-body viscosity leads to a more elongated scission shape, the postscission kinetic energy is also less in this case. These two effects combine to reduce the kinetic energy to the values given by the dashed curve as the two-body viscosity coefficient increases to ∞. As shown in refs. 17 and 18, the experimental kinetic energies are reproduced satisfactorily in terms of two-body viscosity when the viscosity coefficient μ has the value

$$\mu = 0.015 \pm 0.005 \text{ terapoise} = 9 \pm 3 \times 10^{-24} \text{ MeV sec/fm}^3 .$$

This relatively small viscosity is about 30% of the value that is required to critically damp the quadrupole oscillations of idealized heavy actinide nuclei.

Because one-body dissipation leads to a more compact scission shape, the postscission kinetic energy increases in this case. The combined effect of the decreased prescission kinetic energy and increased postscission kinetic energy is a small decrease in the total at infinity, as shown by the solid curve in Fig. 6. This curve, which has been calculated without the adjustment of any arbitrary parameters, reproduces adequately the experimental kinetic energies for the fission of nuclei ranging from ^{80}Sr to $^{278}110$, although the calculated curve systematically overestimates the experimental values for very heavy nuclei by about 4%.

We should note here that the wall formula, eq. (2.11), (derived under the assumption that the relevant bulk of the gas is at rest) becomes inappropriate in the final stages of fission, when a neck has restricted the free passage of particles from one half of the system to the other. The effect of this restriction is that particles bombarding surface elements of, say, the left-hand part of the system, come mostly from this part and are therefore characterized by a leftward drift. The relevant value of $\dot{n}$ for the left half of the system is then no longer the normal surface velocity with respect to the bulk of the whole system (which is at rest), but the velocity with respect to the leftward moving part, which is the one supplying the particles impinging on this part of the surface. When the neck joining the two nascent fragments has become small enough the window formula, eq. (2.17), would become appropriate for describing the dissipative force opposing the separation of the fragments. According to this formula the dissipation goes to zero as the window closes off. By contrast, the indiscriminate use of eq. (2.11) would imply the nonsensical result that the fragments'

translational motions after scission were opposed by a dissipative force. (See section 7 for a generalized wall formula that takes into account translations.) The proper description of the transition region between the regimes when the wall and window formulae are applicable is, naturally, a more difficult problem than either limiting idealization. The present calculations may be considered as an approximation in which a sudden transition from the wall formula to the window formula is made at scission. (The window formula is then used only in the trivial sense of giving zero dissipation for the separation of the fragments.) A better approximation would be to make this transition somewhat earlier, when the window is small (but not zero) or, even better, to make a smooth transition governed in some way by the gradual loss of communication between the two halves of the system. This is a problem for the future, but we wish to warn the reader that the presently calculated fission-fragment kinetic energies are subject to an uncertainty arising from the above schematic treatment of the transition from the wall formula to the window formula at scission. A general formulation of the one-body dissipation theory applicable to this process can be found in ref. 6.

The curves in Fig. 6 are calculated for nuclei along Green's approximation to the valley of β stability,[25] which is adequate for the comparison made here. The results are calculated for most probable dynamical paths corresponding to starting from rest an infinitessimal distance from the macroscopic saddle point. In calculating the prescission paths for one-body dissipation we make the excellent approximation of neglecting the inertia. This means that the

prescission contribution is zero identically for both the solid and dashed curves. For these two cases the postscission kinetic energy is taken equal to the total nuclear plus Coulomb interaction energy at scission, since infinitely viscous fragments separate without changing their shape. (The very small difference between the dashed curve in Fig. 6 and the curve for infinite two-body viscosity presented in refs. 17 and 18 stems from the use there of a slightly different method for calculating the postscission kinetic energy.)

Because nonviscous fission fragments oscillate as they separate, the postscission contribution to their translational kinetic energy is not equal simply to the total interaction energy at scission. Instead, a small portion of this interaction energy is converted during the separation into vibrational energy rather than into translational kinetic energy.

In calculating the nonviscous translational kinetic energy, we represent the fission fragments in terms of two separated spheroids and integrate numerically the postscission equations of motion until the higher multipole corrections to the Coulomb interaction energy are negligible. At this point the sum of the translational kinetic energy and the Coulomb interaction energy is taken to be the final fission-fragment kinetic energy at infinity. The initial conditions for the postscission motion are determined by making continuous the values of r, σ, $\dot{r}$, and $\dot{\sigma}$ at the scission point. This transition at scission from the three-quadratic-surface parametrization to the two-spheroid parametrization introduces a small discontinuity in the various contributions to the total energy.

The curves for nonviscous flow and for infinite two-body viscosity in Fig. 6 are visibly nonlinear in $Z^2/A^{1/3}$, whereas the curve for one-body dissipation is approximately linear. This approximate proportionality to $Z^2/A^{1/3}$ arises because for one-body dissipation the scission shapes are approximately the same for all nuclei and because the major portion of the total interaction energy at scission is the Coulomb interaction energy, which for a given shape is strictly proportional to $Z^2/A^{1/3}$. However, the slope of the curve for one-body dissipation does change slightly, especially for small values of $Z^2/A^{1/3}$, because the kinetic energy must be zero for $Z^2/A^{1/3} = 0$. (This is to be contrasted with many semiempirical treatments of fission-fragment kinetic energies,[26] which would imply a finite kinetic energy for $Z^2/A^{1/3} = 0$.)

In summary, experimental most probable fission-fragment kinetic energies may be reproduced equally well in terms of either two-body viscosity or one-body dissipation. With two-body viscosity, the viscosity coefficient must be adjusted to optimally reproduce the experimental kinetic energies and turns out to be relatively small. For this case, the fragments from the fission of a heavy nucleus have already acquired substantial kinetic energy by the time they reach the scission point, which is moderately elongated. With one-body dissipation there is no viscosity coefficient to adjust and the motion turns out to be dominated by dissipation. In this case the fragments from the fission of all nuclei are barely moving at the scission point, which is relatively compact.

It appears from the above that the decision whether nuclear dissipation is like ordinary two-body viscosity or like the one-body

dissipation considered here (or some combination of the two) will have to be made with reference to additional experimental data and theoretical analysis. An important piece of experimental evidence in this connection is the near-independence of the fission fragment kinetic energies of the nuclear excitation, in the range from zero (spontaneous fission) to 100 MeV and more. Ordinary viscosity is expected to be a sensitive function of the temperature T proportional, for a Fermi liquid, to T^{-2} at low temperatures. In contrast, and in agreement with experiment, one-body dissipation is expected to be nearly independent of temperature, the factor $\rho\bar{v}$ varying only slowly with excitation.

In any case it is possible to say that the one body dissipation formula, eq. (2.11), even though free of adjustable parameters, does not meet with any obvious catastrophe when confronted with experimental data on fission-fragment energies.

On the other hand there are many anticipated corrections to the simple treatment of dissipation described in this section which, taken together, might or might not spoil the present degree of agreement. (These include corrections for surface diffuseness, quantization, symmetries, residual interactions, neck rupture and an improved transition from the wall formula to the window formula near scission.) Still, as things stand, the fission-fragment energies are at the moment reproduced adequately even though the system is highly overdamped and the descent from saddle to scission is slow and creepy. There seems to exist, therefore, a chance of resolving the "viscous-or-non-viscous?" dilemma raised by experimental data on fission and deep inelastic collisions.

We have made some estimates relevant to this problem which we shall present in the next section.

5. ONE-BODY DISSIPATION IN NUCLEAR COLLISIONS

Abundant experimental evidence indicates that heavy nuclei colliding peripherally at energies up to several MeV per nucleon dissipate most of their relative kinetic energy and angular momentum without fusing. A closer analysis of the data suggests that the two nuclei rapidly assume a stuck binary configuration which rotates like an almost rigid body and subsequently divides into fragments with (initially) a very low relative kinetic energy. Hence it is an essential requirement of any theory of nuclear dynamics that it lead to a strong relaxation in the relative degrees of freedom for nuclear collisions. In this section we discuss the application of the one-body dissipation theory to the collisions of heavy nuclei.

For semi-quantitative estimates of the degree of relaxation implied by the one-body dissipation it may suffice to restrict the discussion to the idealized situation where the nuclei are assumed to remain spherical during the collision. This assumption is expected to be strongly violated during the later stages of the collision process when the dynamical development of the intrinsic shape degrees of freedom, such as neck formation and overall elongation, plays an important role, leading to an appreciably lower interaction barrier in the exit channel. Hence the estimates made in the following can only be taken as indicative; in order to obtain more accurate values it is necessary to include to some extent the shape dynamics.

5.1 Simple Estimates

In a peripheral collision the relative velocity u is almost exclusively tangential and the relative kinetic energy $T = \frac{1}{2}\mu u^2$, which is the energy above the potential barrier, mainly derives from the angular motion. (In this section μ stands for the reduced mass.) According to the window formula the rate of energy dissipation is then approximately given by

$$\dot{T} \approx -\frac{1}{4}\rho\bar{v}\, u^2\, \Delta\sigma = -\frac{1}{4}\,\rho\bar{v}\,\frac{2}{\mu}\,T\,\Delta\sigma \quad , \tag{5.1}$$

where $\Delta\sigma$ denotes the effective area of the window between the two nuclei. Since the motion is essentially tangential the initial rate of angular momentum degradation is given by the similar relation,

$$\dot{L} = -\frac{1}{4}\,\rho\bar{v}\,\frac{1}{\mu}\,L\,\Delta\sigma \quad . \tag{5.2}$$

From the above simple expressions it is possible to obtain rough estimates of the degree of relaxation of the relative motion in a given nuclear collision. As an example, consider the case of a ^{86}Kr projectile colliding with a ^{197}Au target. Taking the effective window radius to be $a \approx 3$ fm (which would be appropriate close to contact between the half-density nuclear radii - see ref. 27), we find for the relative rate of energy degradation

$$-\dot{T}/T \approx 0.25 \times 10^{22}\ \text{sec}^{-1} \quad .$$

If the energy dissipation were to proceed at the initial rate (5.1) total relaxation would be achieved after a time τ given by

$$\tau = (\frac{1}{4} \rho \bar{v} \frac{2}{\mu} \Delta\sigma)^{-1} \quad .$$

Although the dissipation rate decreases with time, the quantity τ can be taken as a measure of the time required for a substantial degree of relaxation. In the case of Kr on Au τ comes out to be around 4×10^{-22} sec, which is of the same order as a typical interaction time for a peripheral collision.[28] During the characteristic time τ the relative radius vector between the two nuclei turns through an angle given by

$$\Delta\Theta = \frac{u}{r} \tau = (\frac{2T}{\mu})^{1/2} \frac{\tau}{r} \quad ,$$

where r is the separation between the two nuclear centers. For Kr on Au this is approximately $\Delta\Theta \approx (T/245 \text{ MeV})^{1/2}$, which for a laboratory bombarding energy of 600 MeV gives a result comparable to the values extracted from the experimental data.[28]

5.2 Dynamical Calculations

The method of estimation employed above is obviously a crude one and it is only meant to serve as a rough guideline. More detailed estimates can be obtained by following the dynamical development of idealized collisions.

Let us consider the situation in which the two colliding nuclei (denoted by T and P) are approximated by spheres. Thus the degrees of freedom retained are the relative separation r and orientation Θ of the two nuclei as well as their intrinsic orientations Θ_T, Θ_P ; the neck degree of freedom as well as the mass flow between the nuclei are ignored. This simple parametization allows one to study approximately the dynamical relaxation of the relative degrees of freedom but is of course inadequate to describe the overall shape evolution.

The inertial masses associated with the four degrees of freedom $r,\Theta,\Theta_T,\Theta_P$ are taken as the reduced mass $\mu=mA_TA_P/(A_T + A_P)$, the moment of inertia associated with Θ and the rigid-rotation moments of inertia $I_{T,P} = \frac{2}{5} M_{T,P} R_{T,P}^2$. (Here the mass is $M_{T,P} = mA_{T,P}$ and $R_{T,P}$ is the equivalent sharp nuclear radius.[29])

The two spherical nuclei are subject to the mutual Coulomb and nuclear interactions. The former is taken as $V = e^2Z_TZ_P/r$; it would be easy to modify the potential to take account of the finite extension of the nuclear charge distribution but such a refinement does not seem warranted at present. The nuclear interaction potential is very sensitive to the separation between the two nuclear surfaces and it is necessary to treat this dependence with care. This is accomplished by employing the "Proximity Potential" for the nuclear interaction,[30] given by $V_N = 4\pi\gamma\bar{R}b\,\Phi(s/b)$ where $s = r - C_T - C_P$ is the surface separation, b is the surface width[29] and $\bar{R} = C_TC_P/(C_T + C_P)$; the "central radii"

$C_{T,P}$ are related[29] to the equivalent sharp radii $R_{T,P}$ by $C \approx R - b^2/R$. Moreover, γ is the specific nuclear surface energy and the dimensionless function $\Phi(\zeta)$ is the incomplete integral of $\phi(\zeta)$, the interaction energy per unit area between two flat parallel nuclear surfaces positioned at the separation $s = \zeta b$. The use of the proximity potential rather than one based on the surface energy of sharp surfaces represents an essential improvement and leads to a good account of experimental elastic-scattering and fusion data.[30]

According to the window formula the friction is proportional to the (one-sided) flux of nucleons between the two nuclei. This quantity is as sensitive to the details of the gap between the two nuclei as the static nuclear interaction potential. Consequently we shall replace the simple window formula (2.17) by the proximity-friction formula derived in ref. (27). This formula approximates the one-body friction by a method analogous to that employed for the proximity potential. That treatment leads to the following expression for the dissipation rate.[27]

$$\dot{E} = 2\pi n_o \bar{R} b \quad \Psi(s/b)(2u_{\parallel}^2 + u_{\perp}^2) \quad ,$$

where $n_o = \frac{1}{4}\rho\bar{v}$ denotes, as in Sec. 2.2, the one-sided flux in nuclear matter. The dimensionless proximity flux function $\Psi(\zeta)$, analogous to $\Phi(\zeta)$, is the incomplete integral of the function $\psi(\zeta)$ which is the one-sided flux per unit area between two flat parallel surfaces with

separation $s = \zeta b$. The use of the proximity friction represents a quantitative improvement similar to that of introducing the proximity potential.

We have carried out calculations for a number of target-projectile combinations in order to gain insight into the dynamics of the relaxation produced by the one-body dissipation. As an example we shall discuss the results of ^{86}Kr on ^{197}Au at laboratory bombarding energies of 600, 800 and 1000 MeV.

In Fig. 7 we display as a function of the initial angular momentum ℓ_i the final orbital angular momentum ℓ_f when the two nuclei have separated. It is seen that the main part of the cross section is associated with fully damped events which, in our limited parametrization, means that the velocity mismatch at the window vanishes. In this situation the two nuclei will roll on each other and carry a relative angular momentum equal to $\frac{5}{7}\ell_i$ (ref. 31).

Another way of illustrating the results is to plot the final kinetic energy associated with the relative motion, T_{CM}, as a function of the scattering angle θ_{CM} (in the center-of-mass system). This is done in Fig. 8. The three curves exhibit a characteristic Z-shape which bears a qualitative resemblance to the structures observed experimentally.[28] However, the inclusion of the neck degree of freedom may considerably change the results; in particular the final interaction barrier E_B would be lowered substantially. Hence, no detailed comparison with experiment should be attempted.

The dynamical evolution of the relaxation process is illustrated in Fig. 9 which is a plot of the relative energy T_{CM} versus the

separation r. The interaction potential corresponding to $\ell = 0$ is indicated. The three collisions are represented as dynamical trajectories entering from the right at a level corresponding to the bombarding energy, gradually suffering damping and finally leaving to the right with a substantially reduced energy. The duration of the various parts of the process is illustrated by the black dots which indicate the position at equal time intervals of 10^{-22} sec. The values of the orbital angular momentum attained at the corresponding points in time are indicated. The same initial angular momentum $\ell_i = 220\ \hbar$ was chosen for all three bombarding energies. For comparison at 1000 MeV the value $\ell_i = 280$ was also used; this corresponds to the same impact parameter as for the $\ell_i = 220\ \hbar$ trajectory at 600 MeV. We note that the largest part of the dissipation occurs before the radial turning point is reached; this is evident from the energy as well as from the angular momentum. This makes the radial motion considerably slower on the way out than on the way in; in the case of 600 MeV only a few MeV of radial kinetic energy is present during the reseparation.

Taking the above results at their face value it is evident that the one-body dissipation, as given in terms of the window formula, does indeed lead to a substantial degradation of the relative motion in a nuclear collision. A more refined calculation, with a proper inclusion of the shape degrees of freedom, might reproduce quantitatively the experimental data. On the other hand there is enough uncertainty in the present comparisons that it cannot be ruled out that the window formula, even when refined, is inadequate. Other mechanisms operating during the moment of contact of two nuclear surfaces may be contributing in an essential way to the dissipation of energy.

6. NUMERICAL TESTS OF THE WALL FORMULA

In addition to comparing the one-body dissipation with experimental results on real nuclei (with all of the attendant complexities and ambiguities of interpretation) it is instructive to test the theory of one-body dissipation against simple, well-defined model calculations. In this section we shall present a (far from exhaustive) set of comparisons with numerical computer studies of non-interacting particles bouncing around in a time-dependent deforming container. The motion of the particles is followed either classically or quantally and the calculated increase in the energy of the particles in the course of time is compared with the predictions of the wall formula.

6.1 Classical Results

As a first test we consider periodic multipole distortions around a spherical shape. The container has infinitely hard, perfectly reflecting walls and its time-dependent shape is specified by the radius vector R(t),

$$R(t) = \frac{R_o}{\lambda} \left(1 + \alpha_n(t)\, P_n(\cos\theta)\right) \quad .$$

Here R_o is the radius of the sphere and λ is a normalization factor (a function of time) ensuring that the volume of the container remains constant in time. Furthermore, P_n denotes the usual Legendre polynomial.

The coefficients α_n are chosen to be of the form

$$\alpha_n(t) = \left(\frac{2n+1}{5}\right)^{1/2} \alpha \cos \omega t \qquad (6.1)$$

With this choice of normalization the root-mean-square deviation from the sphere is, for a given α, the same for all multipolarities n (in

the limit of small amplitudes.) This in turn implies that the dissipation rate predicted by the wall formula (2.11) is the same for all values of n and is, as a quick calculation will verify, given by

$$\dot{E}_{wall} = \rho\bar{v} \oint (R_o \dot{\alpha}_n P_n)^2 \, d\sigma$$

$$= \frac{4\pi}{5} \alpha^2 \rho\bar{v} R_o^4 \omega^2 \sin^2 \omega t \quad .$$

Direct integration of this expression leads to the following formula for the excitation energy as a function of time:

$$E_{wall}(t) = \frac{2\pi}{5} \alpha^2 \rho\bar{v} R_o^4 \omega(\omega t - \frac{1}{2} \sin \omega t) \quad . \tag{6.2}$$

This simple prediction can be compared with the results obtained by solving numerically the exact classical equations of motion. For this calculation the initial conditions are taken as a uniform spatial distribution of particles inside the container and a uniform velocity distribution within a sharp Fermi sphere of radius v_F . To facilitate later comparison with quantal calculations a density of four particles per h^3 of phase space is assumed. The actual solution of the dynamical problem is conveniently obtained by using a Monte-Carlo technique, following a sample of individual particles as they move along locally straight trajectories, occasionally acquiring a modified energy and velocity as a result of collisions with the moving container boundary.

Figure 10 shows the calculated results for an amplitude of $\alpha = 0.2$ and a frequency of $\omega = (0.19)\times 10^{22} \text{sec}^{-1}$ (corresponding to the frequency of a quadrupole oscillation of an idealized heavy nucleus).

Of course, the entire classical treatment can be expressed in simple dimensionless form, but to facilitate the comparison later on with the quantal results we make the following specific choices of the parameter values. The radius R_o is taken to be 6.8465 fm, corresponding to a nucleus with 184 particles. The Fermi energy is taken as ε_F = 33.136 MeV, corresponding to a nuclear density described by a nuclear radius constant close to 1.2049 fm and a mean nuclear mass of 938.9 MeV/c^2. Thus we are studying a relatively heavy nucleus oscillating at a relatively low frequency.

The wall formula prediction corresponding to these values is shown as the full curve in fig. 10. We note that the formula gives an excitation per cycle of around 0.6 MeV per particle or some 110 MeV total excitation. This indicates, in correspondence with Section 3, the large absolute magnitude of the dissipation implied by the wall formula.

The classical (Monte Carlo) computer results are displayed for n = 2,4,6. The following features should be noted. For n = 2 there is a large build-up of excitation energy during the first half of the cycle; during the second half a significant fraction (in this case 60%) of this excitation disappears again, leaving the system with a net excitation after the completion of the cycle equal to around half of the value predicted by the wall formula. For n = 4 this appearance of partial reversibility is largely gone and the curve shows a structural similarity with $E_{wall}(t)$ but overshoots by around 40%. For n = 6 the exact classical result follows closely the wall formula. This remains true as one proceeds to n = 8 (not included in the figure).

This at first sight confusing behavior can be qualitatively well understood as a consequence of the symmetry properties of the various shapes considered. It was an important assumption in the derivation of the wall formula that the particles at any time constitute a randomized gas, as would be the case for an irregular container. This assumption may be rephrased as the demand that there be no single-particle constants of motion. Clearly, this requirement is violated if the container possesses special symmetries giving rise to additional constants of motion. In the present case the effect of such approximate symmetries is exhibited in the results for n = 2. For small amplitudes the quadrupole shape is approximately a spheroid which in turn forms a separable problem. The implications of approximate separability will be discussed shortly. At this point we note that as n is increased the shape of the container becomes more and more randomized and thus approaches the conditions for the application of the wall formula. This is demonstrated by the result for n = 6 (and n = 8).

When the single-particle Hamiltonian possesses special symmetries the phase space can be divided into separate regions with no dynamical intercommunication, each region being characterized by a specific value of the additional constant of motion associated with the particular symmetry present. In such cases the dynamical variation of the potential can only lead to randomization of the particle motion within each sub-region separately, and the quantities characterizing the distribution, such as the mean speed $\bar{v}$, may have different values from region to region; the over-all restriction imposed by the volume conservation is in general not sufficient to ensure that these quantities be the same for all

regions of phase space. Hence the system appears as a collection of separate systems which are dynamically independent of each other, except for the constraint imposed by volume conservation. The most striking consequence of this is that the leading, reversible contribution to the energy change in eq. (2.7) will no longer cancel out but may in fact dominate over the second-order dissipative contribution.

The above statements are quite general. In order to illuminate their content we shall examine in some detail the case of a three-dimensional box. While quite simple to treat, this example displays the characteristic features arising from the presence of symmetries. Let the three sides of the box have lengths 2a, 2b, 2c so that the wall velocities are given by $\dot{a},\dot{b},\dot{c}$. The dynamical problem obviously separates into three one-dimensional systems and the over-all volume conservation imposes the constraint that the product abc remain constant in time.

Consider first the motion in the direction parallel to the side of length a. To leading order the particle collision frequency is $\frac{1}{2}\rho\, v_a/a$ and the energy change per collision is $-2mv_a\dot{a}$, so that the rate of change in mean particle energy is given by $\dot{\varepsilon}_a = -m\overline{v_a^2}(\frac{\dot{a}}{a})$. Clearly, this is just the one-dimensional version of the ideal gas law and can be integrated to give a reversible energy as a function of the distortion a. This energy is readily seen to be inversely proportional to the square of the side length a.

From this result it immediately follows that for the three-dimensional box the particle energy has, to leading order, the following reversible dependence on the distortions:

$$\varepsilon(a,b,c) = \frac{\varepsilon_o}{3}\left[(\frac{a_o}{a})^2 + (\frac{b_o}{b})^2 + (\frac{c_o}{c})^2\right] .$$

Here it has been assumed that when the sides are a_o, b_o, c_o the particles are distributed isotropically with a mean energy ε_o. We note in passing that with this assumption we always have $\varepsilon(a,b,c) \geq \varepsilon(a_o,b_o,c_o)$ for distortions that conserve volume.

Now assume that the box is subjected to a periodic volume-conserving distortion of the form

$$a = \ell\, e^{\alpha \cos \omega t} \approx \ell(1 + \alpha \cos \omega t) \ ,$$

$$b = c = \ell\, e^{-\frac{1}{2}\alpha \cos \omega t} \approx \ell(1 - \tfrac{1}{2}\alpha \cos \omega t) \ .$$

Then, to leading order in α, we find for the reversible energy change

$$\Delta\varepsilon(t) = \varepsilon(t) - \varepsilon_o \approx \varepsilon_o\, \alpha^2 (1 - \cos \omega t)^2 \ .$$

This reversible energy (times one half) is displayed in fig. 10 (dashed curve) for a box with the same volume as the sphere considered (i.e. $8\,abc = \frac{4\pi}{3} R_o^3$); the amplitude has been adjusted so as to give the same value for the wall dissipation rate as for the oscillating sphere (which in the present case implies $\varepsilon_o \alpha^2 = 0.3947$ MeV). We see that the bump appearing in this case is somewhat reminiscent of the bump in the excitation curve for the quadrupole oscillation (though it is bigger by a factor of two or three). This fact can be taken as an indication that the latter bump is due to the special (approximate) symmetry of the P_2 distortion, leading to an approximate separability of the equations of motion. As in the case of the box this would invalidate the assumption of the randomization of the motions of the

particles rebounding from variously moving elements of the surface. In going to higher multipole deformations (P_4,P_6,P_8) the regularity of the approximately spheroidal P_2 distortion is lost, the particles become randomized through collisions with the increasingly corrugated surface, and the results of the computer studies support the validity of the wall formula once such randomization is insured.

This interpretation of the results can be further tested by introducing an explicit randomization of the particle motions. Such randomization can be enforced by making the particles jump, after a certain length of travel, to a new random position and take off from there with a new random direction. This is superficially like introducing a finite two-body collision mean free path but it is important to stress that the similarity <u>is</u> superficial. Thus even when the free length of travel is short (e.g. 1 fm) the particles are still completely independent of each other and the behavior of the gas does <u>not</u> approach the hydrodynamic limit of correlated flows that would be expected when the short mean free path is a result of two-body collisions. The introduction of the jumps is just a stratagem to introduce randomization and destroy the particles' long-range memory of the container's shape (including its symmetries).

Figure 11 illustrates the results of such calculations with jumps, for the case of quadrupole oscillations (n = 2). All the parameters of the container and gas are otherwise the same as in Fig. 10. The thick curve labeled ∞ is the same result as in Fig. 10, corresponding to an infinite mean free path (i.e. no jumps). The other thick curve is the prediction of the wall formula, extended now over

two periods of oscillation. The curve labeled 32 corresponds to a mean free path of 32 fm (recall that the radius of the oscillating sphere is about 6.8 fm). The result is not very different from the case of an infinite mean free path. A large reversible bump is again evident, and it is repeated rather faithfully in the second cycle of the oscillation. Going to a mean free path of 16 fm, which is now comparable with the diameter of the container, a dramatic change is seen to occur. The reversible bump in the first cycle has disappeared and in the second cycle a dip has replaced the bump. With the mean free path reduced to 8 fm the dissipation curve is beginning to show a very rough resemblance to the wall formula prediction, and reduction of the mean free path to 4, 2 and 1 fm seems to lead to a converging sequence approaching the wall-formula curve. We have not traced the reason for the apparent convergence to a value possibly a little higher than the solid curve. By and large, however, the conclusion at this stage is that the wall formula, derived originally for a unit area of an infinite plane wall or piston, does represent, at least approximately and for a limited time, the excitation energy fed into a gas of non-interacting classical particles by the moving boundaries for an actual finite container — provided, that is, that the particle motions have sufficient opportunity of becoming randomized, either by corrugations of the boundary of the container or by other randomizing agencies.

6.2 Quantal Results

So far our discussion has been entirely within the framework of classical mechanics. What if the particles in the well are quantized, i.e. if their motions are followed according to the Schrödinger equation

rather than according to classical equations of motion? Will the simple wall formula predictions become completely irrelevant or will they remain qualitatively or even quantitatively useful?

The tools for studying this question were at hand, in the form of a computer program for numerically solving the single-particle Schrödinger equation in a time-dependent Woods-Saxon well.[32] One study along these lines (for a sequence of fissioning shapes) had in fact already been reported[33] and will be discussed presently. In Fig. 12 we show the results of a related study, but for one cycle of a periodic oscillation, similar to those of Fig. 10. The oscillation is now for a hexadecapole mode (n = 4), the frequency is considerably higher ($\omega = 1.08 \times 10^{22}$ sec^{-1}) and the amplitude is somewhat smaller. (The maximum value of α_4 is 0.2 rather than $0.2\sqrt{9/5}$, which would follow from eq. (6.1).) Note that the comparison between classical and quantal calculations is now no longer clear-cut: the classical particles bounce about in a sharp-walled well, whereas the quantized particles move in a diffuse Woods-Saxon well.

The solid curve in Fig. 12 is again the wall formula prediction. The triangles show the result of the classical calculation. These results are now closer to the wall formula than the similar hexadecapole curve in Fig. 10. This might be due to the fact that, because of the higher frequency in Fig. 12, the particles have 5.68 times less time (in one cycle) to explore the shape of the container and to become aware of its remaining regularities.

The (lower) dashed curve represents the excitation energy calculated quantally for a Woods-Saxon well with a diffuseness parameter

a = 0.66 fm (a value characteristic of actual nuclei) and the dot-dashed curve is for a much sharper well with a = 0.1 fm.

Both quantal results are of the order of magnitude of the wall-formula prediction. There appears to be a rather strong dependence of the quantal results on diffuseness (compare ref. 6) and for the sharper of the two Woods-Saxon wells the correspondence with the classical calculations (in a sharp well) and with the wall formula is quite remarkable. It is something to marvel at that the dot-dashed curve required a horrendous numerical solution of the time-dependent Schrödinger equation in two dimensions, for dozens of single-particle wave-functions, whereas the solid line is a back-of-the-envelope calculation resulting in the analytic formula (eq. 6.2)

$$E(t) \approx 1.9 \ (\omega t - \frac{1}{2} \sin \omega t) \text{ MeV}.$$

Lest the reader gain the impression that everything about the problem can be understood on the basis of the wall formula, we present a sequence of figures illustrating that the relation between the quantal, classical and analytic (wall formula) results can be much more complex and is, at the moment, somewhat obscure.

Figures 13-16 refer to the oscillations of an <u>exactly</u> spheroidal well whose equation is

$$\frac{x^2}{a(t)^2} + \frac{y^2}{a(t)^2} + \frac{z^2}{c(t)^2} = 1,$$

where

$$a(t) = R_o(0.8875 - 0.0375 \cos \omega t) \quad ,$$

and

$$a^2 c = R_o^3 \quad .$$

The oscillation is thus about a deformed (prolate) shape with a ratio of axes $c:a = 1.4305$ and the amplitude is fairly small, ranging from $c:a = 1.6283$ at $\omega t = 0$ to 1.2635 at $\omega t = \pi$. The quantal calculations are for particles in a Woods-Saxon well with the above geometrical shape and the classical calculations are for an infinite square well.

In Fig. 13 the frequency is $\omega = 1.52 \times 10^{22}$ sec^{-1} and the different curves have the same meaning as in Fig. 12. We see that for about half a period all four curves are fairly similar. Later the wall formula and the sharper Woods-Saxon quantal results continue to be somewhat similar but the more diffuse Woods-Saxon quantal result falls considerably lower, as does the classical result. In Fig. 14 the frequency is $\omega = 0.76 \times 10^{22}$ sec^{-1}. Here all four curves have about the same magnitude after a quarter of a period, after which the wall formula result is much higher than the others. The more diffuse Woods-Saxon quantal curve and the classical results show a remarkable degree of correspondence. In Fig. 15 the frequency is lowered further to $\omega = 0.38 \times 10^{22}$ sec^{-1}. The classical and more diffuse Wood-Saxon calculations both show a large reversible bump, reminiscent of Fig. 10. This bump dominates also Fig. 16, where the frequency is $\omega = 0.19 \times 10^{22}$ sec^{-1}. In this case the classical result is reversible to an astonishing degree, the excitation at $\omega t = 2\pi$ being zero within the statistics of the Monte Carlo

procedures. The result looks very much like the case of the parallel-sided box discussed earlier. The regularity of the spheroidal potential must again be drastically affecting the motion of the particles. Why the curve for the sharper Woods-Saxon well lies much lower than the others is not clear - but an explanation might be related to the general circumstance that in all the quantal results a new feature of the problem emerges at low frequencies. Thus when the characteristic quantum energy $\hbar\omega$ becomes less than the spacing of the single-particle levels at the Fermi-surface, the excitation energy calculated quantally might be expected to tend to zero rapidly (exponentially) as the adiabatic limit is approached. (Recall the Landau-Zener theory of such processes, ref. 34.) The excitation curve in such cases may be dominated entirely by the approach to each other, during the deformation, of a single pair of levels at the Fermi surface. Such an approach may well occur to a greater extent for one type of well than for another, and the results may differ drastically as one changes the parameters of the well or the number of particles in it. We have indeed verified that the big bump in Figs. 15 and 16 is due to a characteristic near-crossing of a pair of levels, and that the bump may be made to disappear by changing the particle number slightly. We have not, however, pursued the calculations to a point where we would be in a position to give a well-founded interpretation of all the effects involved.

Finally, we show in Fig. 17, based on ref. 33, the result of comparing the wall formula with a quantal calculation for an aperiodic deformation. In this case a diffuse potential well is following a sequence of deformations calculated to be the saddle-to-scission

trajectory for an idealized liquid drop. The size and charge of the drop in the trajectory calculation were taken to represent a nucleus of ^{236}U and a fairly small (ordinary) viscosity of 0.02 terapoise was included (ref. 18). With these parameters (and an initial energy of 1 MeV in the fission direction) the time for the descent from saddle to scission is about 39×10^{-22} sec and the energy dissipated (because of the ordinary viscosity) is about 0.1 MeV per particle. This viscous excitation is plotted as a function of time as the dashed curve in Fig. 17.

The solid curve is the result of applying the wall formula to the relevant sequence of shapes (and carrying out the integrations over the surface and over time numerically). The dotted curve is a free-hand sketch meant as a reminder that the wall formula should not, in fact, continue to be used all the way up to scission, where the topology of the vessel is about to change from a single container to a pair of containers. In the latter case the window formula would be more appropriate (see Section 5). The result would be a dissipation curve with a nearly horizontal slope at scission (the dissipation due to the relative motion of the two fragments tends to zero as the neck between them pinches off). The dotted curve is a qualitative indication that somewhere around $t \approx 31\text{-}36 \times 10^{-22}$ sec (see Fig. 18) such a flattening-out of the one-body dissipation curve might be expected.

The solid and open circles show the results of the numerical quantal calculations. The former give the excitation energy (per particle) taken with respect to the ground state of the system at the time in question. Because of the axial and reflection symmetries of the potential well

this excitation is expected to include a reversible part, resulting from the separability of the problem. (See Section 6.1.) An attempt to estimate the irreversible part of the excitation (which is the part that the wall formula is supposed to estimate) is shown by the open circles. They show the result of subtracting from the total excitation energy the energy of a "pseudo ground state", defined as the state that the system would reach if the deformation were proceeding infinitely slowly. Because of the symmetries present, single-particle levels with different quantum numbers are allowed to cross during the deformation and, even when the rate of deformation is infinitely slow, the system does not arrive at the true ground state appropriate to its instantaneous shape but at a pseudo ground state with higher energy. This excess energy is, however, reversible, since a reversal of the infinitely slow deformation would bring the system back to its original state (because of the allowed level crossings). This reversible energy is just a manifestation of the separability of the problem discussed in Section 6.1 and illustrated there by the box calculation.

The conclusions to be drawn from Fig. 17 seem to be as follows. First, the order of magnitude of the quantal and wall-formula dissipation energies are similar and, perhaps, can even be said to exhibit a semi-quantitative correspondence. Second, for the rate of deformation used in the calculation, the absolute magnitude of the excitation energy would be about $\frac{3}{4}$ MeV per particle, corresponding to a total excitation close to a couple of hundred MeV! This confirms once more the very large absolute magnitude of one-body damping, also when it is treated quantally. (As can be seen by comparison with the dashed curve in

Fig. 17 this damping is an order of magnitude greater than two-body damping associated with a viscosity coefficient of 0.02 terapoise.) This suggests that it would be out of the question for an actual Uranium nucleus to descend from saddle to scission at the rate corresponding to Fig. 17. (At least in the case of fission at moderate energies, when superfluidity and shell effects may be disregarded.) This is, of course, consistent with the results of Section 4, which show that when one-body damping is allowed to determine the dynamics of the saddle-to-scission descent, the process is slow and creepy.

7. GENERALIZED WALL FORMULA AND THE NEW DYNAMICS

In this section we shall first generalize the wall formula (2.11) to the case when the vessel containing the gas may be translating and/or rotating in addition to changing its shape. We shall then discuss the formal structure of the equations of motion for the shape changes of a simply-connected leptodermous system in the case when one-body dissipation dominates the deformations.

7.1 Generalized Wall Formula

In deriving the wall formula (2.11) the bulk of the gas was assumed to be at rest. If the container is endowed with an overall translation or rotation the formula, as it stands, would predict the nonsensical result that even in the absence of any intrinsic changes of shape there would be a steady dissipation associated with pure translations or rotations.

This failure of eq. (2.11) is associated with the fact that a steady translation or rotation of a rigid container would, in practice, set up a drift (with the character of a translation or rotation) in

the bulk of the gas. The relative normal velocity of a surface element with respect to the particles about to strike it would then not be $\dot{n}$, the normal velocity in space of the surface, but $\dot{n}-D$, where D (a function of position on the surface) is the normal component of the relevant drift velocity of the particles about to strike the element of surface in question. If the drift reached a stage where its normal component D was actually equal to the normal surface velocity $\dot{n}$ itself, the pressure change $\rho\bar{v}(\dot{n}-D)$ associated with the motion of the surface element relative to the gas would vanish and the flow of energy from the walls to the particles would cease.

The appearance of a drift in the gas in the case of translations and rotations is associated with the failure of the randomization hypothesis. A translation and/or rotation implies a highly correlated type of motion of the surface elements, and particles in a container that is set into translational and/or rotational motion obviously do not return to their original velocity distribution after a few collisions with the walls but, on the contrary, are rapidly taught to co-translate and/or co-rotate with the container.

In general then the dissipation associated with surface displacements δn proceeding at a rate $\dot{n}$ should be written as

$$\delta E = \rho\bar{v} \oint (\dot{n}-D)\delta n \, d\sigma \quad ,$$

or (7.1)

$$\dot{E} = \rho\bar{v} \oint (\dot{n}-D)\, \dot{n} \, d\sigma \quad ,$$

where D specifies the normal component of the drift velocity of the particles about to strike the surface element $d\sigma$. In the case of a

rigid container endowed with a steady translation with velocity $\vec{V}$ and a steady rotation about an origin 0 with angular velocity $\vec{\Omega}$ the dissipation would cease if the drift became such that

$$D = (\vec{V} + \vec{\Omega} \times \vec{R}) \cdot \vec{n} \quad , \tag{7.2}$$

since this is just the normal velocity $\dot{n}$ of a surface element of the rigidly moving container ($\vec{R}$ is the radius vector from 0 to the surface element in question).

Thus for a rigid container in steady motion the modified wall formula (7.1), with D given by (7.2), correctly predicts the vanishing of energy dissipation.

Now comes the real question: what is the drift distribution D to be inserted in (7.1) when the container is translating, rotating and (slowly) changing its shape?

We shall try to solve this problem by seeking a function D that

a) has as little spatial structure as possible and

b) satisfies a self-consistency constraint and the resulting conservation conditions on linear and angular momentum.

The condition of "least spatial structure" is motivated by the long mean free path aspect of the problem and the assumed irregular shape of the container. This, we feel, makes it impossible for the gas to sustain any intricate velocity distribution patterns, such as arise in the case of normal fluids, where the correlations induced by short mean free paths lead to flow patterns in the bulk (e.g., an irrotational flow pattern). In the case of long mean free paths

any such pattern, even if set up at some instant, would quickly diffuse away through the particles' uncorrelated straight-line motions in the bulk of the gas and the randomizing collisions with the boundary (assumed irregular). The only drift patterns that can survive would seem to be those maintained by the regular, correlated features of the wall motions, namely the features associated with translations and rotations. (We should stress that we are explicitly concentrating our attention in this section on irregularly-shaped vessels whose shapes and motions have no regularities or symmetries other than possible translations and rotations.)

The further (self-consistency) condition that we shall apply to determine D is the requirement that, when the model of a gas in a vessel is used for a self-cohesive system such as a nucleus, there should be no net flow of linear or angular momentum between the gas and the vessel. This is because in this case the vessel is not a material body capable of trading linear and angular momentum with the particles, but merely a self-consistently generated potential well produced by the particles themselves.

Consider then a vessel whose surface $\sum$ at time t is specified by a radius vector $\vec{R}(t)$ taken (for definiteness) from the center of gravity C of the space enclosed by the vessel. The vessel is filled with a gas exerting a (vector) pressure $\vec{p}$ along the normal direction $\breve{n}$ at each point on the surface. The total force $\vec{F}$ and total torque $\vec{T}$ exerted by the gas on the vessel are given by

$$\vec{F} = \oint \vec{p}\, d\sigma \quad , \tag{7.3a}$$

$$\vec{T} = \oint \vec{R} \times \vec{p}\, d\sigma \quad . \tag{7.3b}$$

The work done by the container on the gas when the surface elements are displaced from $\vec{R}$ to $\vec{R} + \delta\vec{R}$ is

$$\delta E = -\oint \vec{p} \cdot \delta\vec{R} = -\oint p\delta n \quad , \tag{7.4}$$

where p is the magnitude of $\vec{p}$ and δn is the normal component of the displacement $\delta\vec{R}$ of a surface element.

For a real two-component system, consisting of a gas and a material vessel, the total force $\vec{F}$ and torque $\vec{T}$ may or may not vanish (e.g., if p is a constant then $\vec{F}$ and $\vec{T}$ vanish but, for some arbitrary distribution of the pressure, $\vec{F}$ and $\vec{T}$ would, in general, not be zero). However, as noted above, when we use the model of a vessel filled with a gas to represent a single system, such as a nucleus, where the vessel is merely the potential well generated by the particles, we must insist that $\vec{F}$ and $\vec{T}$ vanish identically (otherwise the particles of the model nucleus, even when left to themselves in force-free space, could start moving spontaneously, their linear and angular momenta changing in time). The vanishing of eqs. (7.3a) and (7.3b) thus imposes two conditions on the admissible expressions for the pressure $\vec{p}$. With the pressure written as

$$\vec{p} = \frac{1}{3}\rho\overline{v^2}\,\breve{n} - \rho\bar{v}(\dot{n} - D)\,\breve{n} + \ldots$$

(compare eq. 2.6) these become conditions on the drift pattern D:

$$\oint (\dot{n}-D)\, \breve{n}\, d\sigma = 0 \quad , \tag{7.5}$$

$$\oint \vec{R}\times\breve{n}\, (\dot{n}-D)\, d\sigma = 0 \quad , \tag{7.6}$$

or

$$\oint \dot{q}\, \breve{n}\, d\sigma = 0 \quad , \tag{7.7}$$

$$\oint \vec{R}\times\breve{n}\, \dot{q}\, d\sigma = 0 \quad , \tag{7.8}$$

where $\dot{q}$ stands for the relative normal velocity:

$$\dot{q} \equiv \dot{n}-D \quad . \tag{7.9}$$

We shall now incorporate our "least structure" requirement on D by trying the following two-parameter functional form for D:

$$D = (\vec{V} + \vec{\Omega}\times\vec{R})\cdot\breve{n} \quad . \tag{7.10}$$

Thus we shall assume that also in the general case the functional form of D is that associated with a translation $\vec{V}$ and a rotation $\vec{\Omega}$ (about the center of mass C), the vectors $\vec{V}$ and $\vec{\Omega}$ being parameters to be determined presently. This is done by inserting (7.10) into (7.5) and (7.6), which leads to

$$\oint [\dot{n} - (\vec{V} + \vec{\Omega}\times\vec{R})\cdot\breve{n}]\breve{n}\, d\sigma = 0 \quad , \tag{7.11}$$

$$\oint (\vec{R}\times\breve{n})[\dot{n} - (\vec{V} + \vec{\Omega}\times\vec{R})\cdot\breve{n}]\, d\sigma = 0 \quad . \tag{7.12}$$

These are two linear equations for the time-dependent vectors $\vec{V}(t)$, $\vec{\Omega}(t)$, the coefficients in the equations being given in terms of the configuration of the surface, specified by $\vec{R}$, and its state of motion, specified by $\dot{n}$. As we shall show the solution of equations (7.11), (7.12) has a relatively simple geometrical interpretation. To see this denote the configuration of a deforming surface at time t by $\sum(t)$ and at time $t + \delta t$ by $\sum(t + \delta t)$. Suppose one wishes to make the best possible fit to the new surface $\sum(t + \delta t)$ by taking the old surface $\sum(t)$ and rigidly translating it by some distance and rotating it by some angle about its center C. It turns out (see below) that if for the translation one takes $\vec{V}\delta t$ and for the rotation one takes $\vec{\Omega} \times \vec{R}\ \delta t$, where $\vec{V}$ and $\vec{\Omega}$ satisfy (7.11) and (7.12), the fit to the surface $\sum(t + \delta t)$ will be optimal in the sense of a least-squares adjustment of the integrated normal distance between the two surfaces.

To verify this define a quantity $\dot{Q}$, proportional to the surface integral (divided by $(\delta t)^2$) of the square of the normal distance between the surface $\sum(t + \delta t)$ and the translated and rotated surface $\sum(t)$. Thus

$$\dot{Q} \equiv \rho\bar{v} \oint d\sigma\ [\dot{n} - (\vec{V} + \vec{\Omega} \times \vec{R}) \cdot \breve{n}]^2$$

$$= \rho\bar{v} \oint d\sigma\ \dot{q}^2 \quad .$$

(The factor $\rho\bar{v}$ is included to bring out the similarity of $\dot{Q}$ and $\dot{E}$.) If $\dot{Q}$ is to be stationary with respect to variations $\delta_{\vec{V}} \dot{Q}$, $\delta_{\vec{\Omega}} \dot{Q}$ associated

with arbitrary changes $\delta\vec{V}$ and $\delta\vec{\Omega}$ we must have

$$\delta_{\vec{V}} \dot{Q} = \rho\bar{v} \oint d\sigma \; 2\dot{q}(-\delta\vec{V} \cdot \breve{n}) = 0$$

and

$$\delta_{\vec{\Omega}} \dot{Q} = \rho\bar{v} \oint d\sigma \; 2\dot{q}(-\delta\vec{\Omega} \times \vec{R} \cdot \breve{n}) = 0 \quad ,$$

or

$$\oint \dot{q}\breve{n} \, d\sigma = 0$$

and

$$\oint \vec{R} \times \breve{n} \, \dot{q} \, d\sigma = 0 \quad .$$

Now these are precisely the equations (7.11), (7.12), which proves that for the $\vec{V}$ and $\vec{\Omega}$ deduced from these equations, the value of $\dot{Q}$ would be stationary (in fact a minimum). We shall refer to the $\vec{V}(t)$ and $\vec{\Omega}(t)$ obtained by solving equations (7.11) and (7.12) as the "instantaneous (rigid-motion) tracking parameters" of the deforming shape $\sum(t)$.

Thus we have the following theorem: "The least-structured drift pattern (i.e a rigid-motion type of pattern described by $(\vec{V} + \vec{\Omega}\times\vec{R}) \cdot \breve{n}$) that ensures conservation of linear and angular momentum of a gas in a moving and deforming container is such that $\vec{V}$ and $\vec{\Omega}$ are the instantaneous tracking parameters of the container's motion." We may now write the generalized wall formula for the rate of energy dissipation that follows from eq. (7.4) as

$$\dot{E} = \rho\bar{v} \oint \dot{q}\dot{n} \, d\sigma = \rho\bar{v} \oint [\dot{n} - (\vec{V} + \vec{\Omega} \times \vec{R}) \cdot \breve{n}] \, \dot{n} \, d\sigma \quad , \tag{7.13}$$

where $\vec{V}, \vec{\Omega}$ are the instantaneous tracking parameters defined above. They

are functions of the configuration and its state of motion, as given by equations (7.11) and (7.12). Note that in virtue of these equations the value of $\dot{E}$ may also be written as

$$\dot{E} = \rho\bar{v} \oint [\dot{n} - (\vec{V} + \vec{\Omega} \times \vec{R}) \cdot \breve{n}]^2 \, d\sigma = \dot{Q} \quad . \tag{7.14}$$

The rate of dissipation $\dot{E}$ in eq. (7.13) is a definite (though implicit) function of the configuration of the surface and its state of motion. The Rayleigh dissipation function (in terms of which equations of motion in generalized coordinates for dissipative systems are commonly derived) is one-half of this function $\dot{E}$.

The generalized wall formula (7.14) has now manifestly no problems as regards conservation of linear or angular momenta for steady translations or rotations. Also the energy dissipation vanishes for such steady motions. Some misunderstandings in this respect seem to have arisen with reference to the wall formula (2.11) because it was sometimes not stressed sufficiently that eq. (2.11) was derived for a gas assumed to be at rest, with no macroscopic drifts present. In this connection we might dispose of another misunderstanding, revealed by discussions with our colleagues, according to which the one-body dissipation, depending as it does on the relative normal velocity of the fluid and the neighboring surface element, would have to vanish identically because of the (hydrodynamical) boundary condition which demands that the particle flux across the moving boundary, and thus the normal relative velocity, vanish. The important thing to remember in this connection is that the pressure expression (governing the rate of energy dissipation) is given in terms of the surface velocity relative to the drift velocity characteristic of the

particles about to strike it, whereas the average local mass flow of the fluid is given in terms of the drift velocity of all particles in a given volume element. There is then nothing inconsistent in having one drift for particles about to strike an element of surface (such that the surface is in motion with respect to this drift) and another drift for the total mass flow of all particles near the surface, such that this mass flow follows the boundary, without violating the proper boundary condition. The simple example of a piston moving into a cylinder filled with an (originally) stationary long-mean-free-path gas illustrates this point. The drift velocity of the gas is (originally) zero and the piston moves with respect to (the drift of) the particles about to strike it. But the region close to the advancing piston contains both the particles about to strike it and the particles that have just re-bounded, whose speeds have been increased by the collision. In the region of space close to the piston there is, therefore, a net drift in the direction of the piston's motion, which is in fact just sufficient to keep vacating the space claimed by the piston and to satisfy the no-flux boundary condition.

Figure 19a illustrates the situation in velocity space. It is similar to Fig. 1 and gives the velocity distribution for particles in the immediate vicinity of the advancing piston. For ease of illustration we consider the velocity distribution function f(v) of the undisturbed gas in the cylinder to be a Fermi function with Fermi velocity v_F, indicated as a sphere centered on the point 0 in Fig. 19. This point corresponds to the origin of a reference frame in which the undisturbed gas is at rest. The point 0' locates the (negative) normal velocity

of the piston as seen from such a frame. The particles which have just collided with the piston have had their z-components of velocity with respect to the piston reversed, and are therefore bounded by (a portion of) a sphere centered on 0'', where 0'' 0' is equal to 0'0.

The velocity distribution of the particles in the immediate vicinity of the piston is zero outside the reflection symmetric boundary in Fig. 19a and constant inside. (The constancy of the distribution function is an immediate consequence of Liouville's theorem and may be verified by a trivial calculation of the collision kinematics. In particular there is no doubling of the velocity distribution function in what would be the overlap region of the two Fermi spheres. Note also that since a general velocity distribution f(v) can be considered as made up of stacks of step-like Fermi distributions with different radii v_F, the generalization of Fig. 19a is obvious and consists of stacking up distributions similar to Fig. 19a but with a variety of values of v_F.)

It is clear now that even though particles about to strike the piston (those to the right of the dashed line in Fig. 19a) are characterized by a velocity drift of magnitude 0'0 with respect to the piston, the drift of all particles with respect to the piston is zero, because of the reflection symmetry about 0'. It is also clear that because of this symmetry there is no flux of particles through the moving piston, so that the continuity condition at the piston is satisfied. We note, however, that the volume of the distribution in Fig. 19a is greater than the volume of a single sphere of radius v_F. Since (again by Liouville's theorem) the density of representative

points in phase space is fixed, it follows that the particle density in real space must have increased in the vicinity of the piston. This density pile up increases with the speed of the piston, reaching a limiting value of a factor of two when the piston speed exceeds the velocity v_F. (Fig. 19b.) If the piston were receding, the boundary in velocity space would be as shown in Fig. 19c, and the particle density near the piston would have decreased. For a piston receding with a speed exceeding v_F the volume in Fig. 19c would vanish and the density would be zero, as one would expect.

From the above discussion it is clear that the motion of the surface elements of a deforming vessel must induce density changes (near the surface) away from the average density ρ, but that this is not inconsistent with the hypothesis that (because of the randomization of the particles' motions) the effective density of the particles about to strike the surface continues to be characterized by ρ. The continued use of the wall formula (2.11) with a fixed average value of ρ may then be justified to the extent of the validity of the randomization hypothesis.

The reason for the original misunderstanding concerning the boundary condition is that in conventional (short-mean-free-path) fluid mechanics one does not make a distinction between the drift of particles about to hit an element of surface and the total drift. Because of the short mean free paths a single local drift is assumed to characterize each point in space and the velocity distribution at any point in space is always assumed to be spherically symmetric about the local drift velocity. Distributions like Fig. 19 are not contemplated in short-path fluid mechanics.

The situation is different in the case of long mean free paths and a careful distinction should be made between the drift of particles about to hit the surface and the total drift. This is also the reason why in this section we were careful to refer to D as the normal drift component of particles about to hit an element of surface located by the vector $\vec{R}$, without implying that the total drift at $\vec{R}$ is $\vec{V}+\vec{\Omega}\times\vec{R}$. There is similarly no implication that the total drift at a point $\vec{r}$ in the bulk is $\vec{V} + \vec{\Omega}\times\vec{r}$.

7.2 Equations of Motion

In order to derive the general equations of motion of a system experiencing one-body dissipation we need, in addition to the Rayleigh dissipation function given as one-half of $\dot{E}$ in eq. (7.14), the potential and kinetic energies of the system, expressed in terms of its configuration and state of motion. In the case of the kinetic energy this calls for an analysis of the collective drift of the particles in the bulk of the system (and not only of the normal surface component D of the particles about to strike the surface).

Insofar as the system is dominated by dissipation a plausible hypothesis would seem to be that the kinetic energy would have the same form as for a very viscous body, i.e. that as regards translations and rotations the system behaves like an (almost) rigid body and that as regards intrinsic changes of shape the kinetic energy associated with these changes is negligible. The equations of motion for the translation and orientation degrees of freedom would then presumably be the familiar equations for an asymmetric top (with a slowly varying inertia tensor) and for the intrinsic changes of shape they would be

first order equations (without an inertial term) balancing conservative and possibly centrifugal (but not Coriolis) forces against dissipative forces.

We have so far not been entirely successful in writing down the general equations embodying the above hypothesis and in what follows we shall only illustrate the structure of the equations of motion governing intrinsic changes of shape in the case when the angular momentum is zero and the problem of rotational degrees of freedom does not arise.

Consider for definiteness a leptodermous, incompressible system such as an idealized nucleus, whose potential energy, apart from a constant volume term, consists of a surface energy E_s associated with a surface tension γ and a Coulomb energy E_c due to a uniform charge density ρ_e. The change in the total energy associated with a surface displacement specified by normal deformations δn is, by well-known theorems (ref. 35), given by the following surface integral

$$\delta E = \delta E_s + \delta E_c$$

$$= \oint (\gamma\kappa + \frac{1}{2}\rho_e\phi)\ \delta n\ d\sigma \quad ,$$

where κ is the total curvature of the surface and ϕ is the electric potential at the point in question. The quantity $\gamma\kappa + \frac{1}{2}\rho_e\phi$ thus plays the role of a generalized force for each element of surface $d\sigma$, such that this force times the displacement δn of $d\sigma$ gives the contribution to the total energy associated with $d\sigma$. As remarked in Section 2, the dissipative force opposing the motion of a surface element $d\sigma$ is,

according to the wall formula, equal to $-\rho\bar{v}\dot{n}$ (when no drifts are present). In order for these forces to balance (recall that we are disregarding the inertial resistance to the motion) the sum must be zero. More precisely, if only volume-preserving displacements are contemplated, it is sufficient that the sum of the forces at each point be a constant independent of position on the surface. Thus

$$\gamma\kappa + \frac{1}{2}\rho_e\phi - \rho\bar{v}\dot{n} = \text{constant} \quad . \tag{7.15}$$

(This is because the expression $\oint$ (const) $\delta n d\sigma$ is identically zero for volume-preserving deformations.)

The constant in eq. (7.15) (a Lagrange multiplier) is readily determined by subtracting from eq. (7.15) its surface average. This gives

$$\gamma(\kappa-\bar{\kappa}) + \frac{1}{2}\rho_e(\phi-\bar{\phi}) - \rho\bar{v}\,\dot{n} = 0 \tag{7.16}$$

(The average of $\dot{n}$ for a volume-preserving displacement is zero.) Hence

$$\frac{dn}{dt} = \frac{1}{\rho\bar{v}}(\Phi - \bar{\Phi}) \quad , \tag{7.17}$$

where Φ is the total generalized conservative force acting on a surface element, and $\bar{\Phi}$ is its surface average. (In the illustrative example used above $\Phi - \bar{\Phi}$ may be re-written as[35]

$$\gamma\kappa_o\left[\left(\frac{\kappa}{\kappa_o} - B_s\right) + 5x\left(\frac{\phi}{\phi_o} - B_c\right)\right] \quad ,$$

where κ_o is the total curvature and ϕ_o is the electric surface potential of the spherical shape, B_s and B_c are the surface and Coulomb energies in units of their values for the sphere, and x is the fissility parameter defined in connection with eq. (3.3).) In any case the content of eq. (7.17) is the simple statement that the rate of displacement of a surface element is equal to the effective driving force $\Phi - \bar{\Phi}$ divided by the dissipation coefficient $\rho\bar{v}$. The relation (7.17) is a first-order equation, so that the configuration of the system at one instant (without regard to the initial velocities) determines the subsequent motion. In a numerical step-by-step solution of eq. (7.17) one could, for example, calculate the normal displacements δn in a time δt by

$$\delta n = \frac{1}{\rho\bar{v}} (\Phi - \bar{\Phi}) \, \delta t \quad ,$$

the right-hand side being a quantity calculable in terms of the configuration in question.

The equation of motion (7.17), even though specialized to non-rotating systems, serves to illustrate the relative simplicity of the smooth background equation of the "New Dynamics" that arises when the motion is dominated by one-body dissipation. This simplicity, as compared to ordinary (e.g. nonviscous) hydrodynamics, is twofold. First, the equation of motion is of first rather than second order. Moreover, the degrees of freedom of an idealized leptodermous nucleus are contained in the specification of the surface only, and not in the specification of a bulk velocity flow pattern. (The degrees of freedom are thus doubly rather than triply infinite.)

7.3 Comments

We shall end this Section with several comments on the relation of the one-body dissipation theory to other discussions of the nuclear problem. First we note that the Time-Dependent Hartree-Fock treatment of a nucleus is a theory of the one-body type, in which the nucleons are independent except through their interactions with a common one-body potential. The TDHF theory is, in addition, explicitly self-consistent: the potential well is not an external container but is generated by the nucleons themselves. Numerical TDHF calculations could thus explore the shortcomings of the one-body dissipation theory described in the present paper arising from the disregard (except for the conservation conditions imposed in Section 7.1) of self-consistency. In addition such calculations could test the degree of validity of the smooth dynamics, suggested in Section 7.2, as regards the effects of quantization, symmetries and small particle numbers. If TDHF calculations could be performed for relatively large systems, devoid of symmetries and/or excited to temperatures where shell effects are suppressed, one might look for quantitative agreement with the predictions of the smooth macroscopic dynamics (unless the self-consistency problem was a crucial one.) For smaller systems at low temperatures drastic modifications might be expected. (Some caution may be necessary in such comparisons in connection with the strictly single-determinant nature of TDHF calculations. The full implications of this feature of the TDHF theory is not clear to us.)

As regards the relation of the present work to the diffusion-type treatments of heavy-ion collisions, one suspects the existence of intimate connections between the two. For example, in the discussion of the window

formula drag between two nuclei, the underlying mechanism is the exchange, back and forth, of nucleons. If this exchange is assumed to have the properties of a statistical random walk, the width of the mass distribution of the fragments is expected to be related to the square root of the number of steps in the random walk, i.e. to the number of exchanges of nucleons through the window. Since this number of exchanges governs the drag between the nuclei, there should be a definite correlation between the variance of the fragment mass distribution and the energy loss in grazing and deep-inelastic collisions. Studies of such correlations are reported in ref. 37.

The intimate relation between the dissipation-dominated dynamics envisioned in the present paper and diffusion-type theories is also illustrated by the qualitative observation that in both cases the time-development of nuclear shapes is expected to be slow and creepy. Such a slow and creepy time development in the context of nuclear fission had been anticipated many years ago by P. Fong[38] and had been a constant theme in his statistical treatment of fission. The equations of our smooth dynamics suggest a quantitative way of describing the saddle-to-scission stage of the process, a problem that is left open in the above treatment of fission.

8. SUMMARY AND OUTLOOK

The situation suggested by this study appears to be as follows.

By taking at face value the independent-particle model of nuclear structure, also when the nuclear potential well is a slowly varying function of time, one is led to suspect that macroscopic nuclear dynamics might often be dominated by dissipative effects. A "randomization hypothesis" leads to two particularly simple dissipation expressions, the wall formula and the window formula. The fundamental time unit for energy dissipation implied by these formulae turns out to be the relatively short single-particle transit time $R/\bar{v}$ (in order of magnitude). The wall formula, when applied to the description of nuclear fission, does not lead to serious disagreement with experiment. The window formula, when applied to nucleus-nucleus collisions, implies a fairly rapid dissipation of the energy of relative motion, but whether there is quantitative agreement or not with experimental data is not certain.

Further theoretical studies (both those reported here and those in ref. 6), bring out the expected failure of the randomization hypothesis for nuclear shapes and motions characterized by special regularities and symmetries. Quantal effects also set a limit to the applicability of simple macroscopic formulae, especially for small systems at low temperatures. Finally at high temperatures approaching the Fermi energy, the independent-particle model and the associated dissipation formulae are expected to break down, the nuclear medium becoming more like an ordinary fluid (which, however, is still expected to be dominated by viscosity - see Section 3).

Taking a broad view of the situation, the following features appear to emerge. A two-part approach to nuclear dynamics, in which effects of shell structure are added to a smooth background, somewhat analogous to the two-part approach to nuclear statics,[36] should be useful. Apart from super-fluidity at very low nuclear excitations, the smooth background dynamics would appear to be characterized by super-viscidity, i.e., a pronounced dominance of the motions by dissipative effects. At moderate temperatures, in the domain of the approximate validity of the independent-particle model, the dissipation is probably largely of the one-body kind, presumably giving place to more conventional two-body viscosity at high temperatures. This smooth dynamics (whose key equations are relatively simple, especially in the one-body domain) is expected to be modified more or less drastically at moderate and low temperatures by symmetries and quantal features.

The future development of macroscopic nuclear dynamics might thus be found to parallel the development of macroscopic nuclear statics. There, the simple smooth background equations for the macroscopic nuclear potential energy (written down in the thirties) were followed (in the sixties) by a gradual understanding of the special effects of symmetries and quantization.

Acknowledgements

The authors are happy to acknowledge instructive discussions with many colleagues at their several home institutions and especially valuable comments from G. Bertsch, H. Flocard, D. Gross, J. Lindhard and W. D. Myers. Three of us (J.B., Y.B. and J.R.) would like to acknowledge the hospitality of the Theory Group in the LBL Nuclear Science Division.

REFERENCES

1. J. H. Jeans, "The Dynamical Theory of Gases", Fourth Edition, Cambridge University Press, 1925.

2. D. Gross, Nucl. Phys. A240, 472 (1975); G. Wegmann, Phys. Lett. 50B, 327 (1974); Nucl. Phys. A251, 289 (1975); Proc. Int. Hirschegg Workshop III, 28 (1975).

Earlier accounts of some of the work described in the present paper can be found in refs. 12 and 15 and in J. Blocki, Y. Boneh and J. Randrup, LBL-5075, 322 (1975); J. Blocki, J. Randrup, M. Robel and W. J. Swiatecki, LBL-5075, 322 (1975); Y. Boneh, J. Blocki and W. D. Myers, LBL-5075, 325 (1975); LBL-5075, 327 (1975); J. Randrup, Proc. Int. Hirschegg Workshop IV, 69 (1976); Y. Boneh, J. Blocki and W. D. Myers, Proc. Int. Hirschegg Workshop IV, 77 (1976); W. D. Myers, J. Randrup and R. Hatch Proc. Int. Hirschegg Workshop IV, 86 (1976); S. Koonin, Proc. Int. Hirschegg Workshop V, 107 (1977); J. Randrup, Proc. Int. Hirschegg Workshop V, 115 (1977).

3. M.H.C. Knudsen, "The Kinetic Theory of Gases", New York, Wiley, 1950.

4. I. L. Bekarevich and I. M. Khalatnikov, Sov. Phys. JETP 12, 1187 (1961).

5. P. Ehrenfest, Annalen der Physik 36, 91 (1911); 51, 327 (1916-17).

6. S. E. Koonin, R. L. Hatch and J. Randrup, Nucl. Phys. A283, 87 (1977); 509; S. E. Koonin and J. Randrup, Nucl. Phys. A (1977) in press; J. Randrup, V. M. Kolomietz and S. E. Koonin, in preparation; J. Randrup, Nordita preprint NORDITA-77/26 (1977).

7. W. J. Swiatecki, Journal de Physique, Supplement No. 8-9, 33, p. C5 (1972).

8. A. Bohr and B. R. Mottelson, "Nuclear Structure", Vol. II, W. A. Benjamin, Inc., 1975, Appendix 6A, p. 655.

9. H.H.K. Tang and C. Y. Wong, J. Phys. A7, 1038 (1974).

10. R. W. Hasse, Annals of Physics 93, 68 (1975).

11. G. D. Westfall et al., Phys. Rev. Letters 37, 1202 (1976); J. Gosset et al., Lawrence Berkeley Lab. Report LBL-5820, May 1977, submitted to Phys. Rev. C.

12. W. J. Swiatecki, Proc. Int. School-Seminar on Reactions of Heavy Ions with Nuclei and Synthesis of New Elements, Dubna, Sep. 23-Oct 4, 1975, p. 89; Lawrence Berkeley Lab. Report LBL-4296 (1975).

13. W. D. Myers and W. J. Swiatecki, Ark. Fys. 36, 343 (1967).

14. L. G. Moretto and R. Schmitt, Jour. de Physique, Colloque C5, Suppl. to No. 11, Vol. 37, C5-109 (1976).

15. A. J. Sierk and J. R. Nix, Proc. Argonne Symp. 1976, Argonne National Lab. Report ANL/PHY-76-2, Vol. 1, p. 407

16. See Ref. 23, p. 366.

17. K.T.R. Davies, S. E. Koonin, J. R. Nix, and A. J. Sierk, in Proceedings of the International Workshop III on Gross Properties of Nuclei and Nuclear Excitations, Hirschegg, Kleinwalsertal, Austria, 1975, edited by W. D. Myers [Technische Hochschule Darmstadt Report No. AED-Conf-75-009-000, 1975], p. 8 .

18. K.T.R. Davies, A. J. Sierk, and J. R. Nix, Phys. Rev. C13, 2385 (1976).

19. H. Goldstein, "Classical Mechanics" (Addison-Wesley, Reading, 1959), Chap. 1, Sec. 5, pp. 19-22.

20. H. J. Krappe and J. R. Nix, in "Proceedings of the Third International Atomic Energy Agency Symposium on the Physics and Chemistry of Fission," Rochester, New York, 1973 (International Atomic Energy Agency, Vienna, 1974), Vol. I, p. 159.

21. J. R. Nix and A. J. Sierk, Phys. Scr., 10A, 94 (1974).

22. J. R. Nix, Nucl. Phys. A130, 241 (1969); Lawrence Berkeley Lab Report No. UCRL-17958, 1968.

23. H. Lamb, "Hydrodynamics" (Dover, New York, 1945), 6th ed., Sec. 329, pp. 579-581.

24. W. D. Myers, Nucl. Phys. A204, 465 (1973).

25. A.E.S. Green, "Nuclear Physics" (McGraw-Hill, New York, 1955), pp. 185, 250.

26. V. E. Viola, Jr., Nucl. Data A1, 391 (1966).

27. J. Randrup, "Nuclear One-Body Proximity Friction", Nordita Preprint 77/7 (1977), to be published.

28. P. Russo et al., Nucl. Phys. A281, 509 (1977).

29. W. D. Myers, Nucl. Phys. A204, 465 (1973).

30. J. Blocki et al., Lawrence Berkeley Lab. Report LBL-5014, 1976; Annals of Physics 105, 427 (1977).

31. C. F. Tsang, Proc. 27th Nobel Symposium, Ronneby, June 11-14, 1974, Physica Scripta 10A, 90 (1974).

32. Y. Boneh and Z. Fraenkel, Phys. Rev. C10, 893 (1974).

33. Y. Boneh, J. P. Blocki and W. D. Myers, Lawrence Berkeley Lab. Report LBL-4397, 1976; Physics Letters 63B, 265 (1976).

34. For example, L. D. Landau and E. M. Lifshitz, "Quantum Mechanics, Non-Relativistic Theory", Pergamon Press, 1965, p. 329.

35. W. J. Swiatecki, Phys. Rev. 104, 993 (1956), especially pp. 996-998.

36. For example, M. Brack et al., Rev. Mod. Phys. 44, 320 (1972). W. D. Myers, Proc. Mont Tremblant Int. Summer School on "The Dynamic Structure of Nuclear States", Mont Tremblant, Canada, 1971; Lawrence Berkeley Lab Report LBL-209; W. D. Myers and W. J. Swiatecki, Nucl. Phys. 81, 1 (1966).

37. W. U. Schröder and J. R. Huizenga,"Damped Heavy Ion Collisions", University of Rochester preprint UR-NSRL-144, March 1977, to appear in Ann. Rev. Nucl. Science Vol. 27; R. Vandenbosch, private communication and University of Washington Nuclear Physics Lab. Annual Report, June, 1977.

38. P. Fong, "Statistical Theory of Nuclear Fission", New York, Gordon & Breach, 1969.

FIGURE CAPTIONS

Fig. 1 Distribution function in velocity space for particles about to strike an element of area $\Delta\sigma$, as seen from a coordinate system moving with $\Delta\sigma$. The z-direction is along the normal to $\Delta\sigma$. The velocities of the mass points cluster symmetrically about the relative gas drift velocity $\vec{U}$, whose magnitude in the z-direction is U_z and whose component in the transverse direction is $\vec{U}_\perp$. A typical particle has velocity $\vec{v}$, with a z-component $v_z\breve{z}$. The average velocity of particles in a slab dv_z is $\vec{U}_\perp + v_z\breve{z}$, and the number of such particles is proportional to the projected distribution function $g(v_z)$.

Fig. 2 The region of integration in the space of ℓ (the distance of a slab of particles from the surface) and v_z (normal component of a particle's velocity). The projected distribution function $g(v_z)$ in the integrand is indicated.

Fig. 3 Two systems in relative motion and communicating through a small window $\Delta\sigma$. The particles about to traverse the window from A to B are characterized by a drift velocity with respect to the window given by $\vec{U}$, and the particles about to go from B to A are characterized by a velocity $\vec{U}'$.

Fig. 4 Dynamical paths in r-σ space of a ^{236}U nucleus from its macroscopic saddle point to scission. The reference path for nonviscous flow is given by the dot-dashed curve. The dashed curves show the paths calculated in ref. 18 for various values of the two-body viscosity coefficient μ, which is measured in

units of terapoise (1 TP = 10^{12} dyn sec/cm^2 = 6.24 × 10^{-22} MeV sec/fm^3). The solid curve shows the path for the one-body dissipation considered here. The scission points are indicated by the tips of the arrowheads.

Fig. 5 Effect of dissipation on scission shapes for the fission of four nuclei. The reference shapes for nonviscous flow are given in the first column. The second column shows the scission shapes for infinite two-body viscosity, and the third column those for the one-body dissipation considered here.

Fig. 6 Comparison of calculated and experimental most probable fission-fragment kinetic energies as a function of $Z^2/A^{1/3}$. The kinetic energies calculated for nonviscous flow are given by the dot-dashed curve. The dashed curve shows the results for infinite two-body viscosity, and the solid curve shows the results for the one-body dissipation considered here. The experimental data are for cases in which the most probable mass division is into two equal fragments; the open symbols represent values for equal mass divisions only and the solid symbols represent values averaged over all mass divisions. The original sources for the experimental data are given in ref. 18.

Fig. 7 The final orbital angular momentum as a function of the initial angular momentum for an idealized ^{86}Kr nucleus bombarding an idealized ^{179}Au nucleus at laboratory energies of 600, 800, and 1000 MeV. The window formula, in the form of the Proximity Friction, was used to describe the dissipation of energy. The value $\ell_f = \frac{5}{7}\ell_i$ corresponds to the rolling condition which, within the

limitations of the model, corresponds to total relaxation in the relative angular degree of freedom. A large part of the cross-section is seen to correspond to such a relaxed situation.

Fig. 8 Energy vs angle plots (Wilczyński diagrams) for the idealized collision of ^{86}Kr on ^{179}Au at three (lab) energies. The labels on the circled points give the final orbital angular momentum appropriate to the angle and energy indicated. The interaction barrier E_B (the same, in the model used, for the entrance and exit channels) is indicated.

Fig. 9 Relative center of mass energy E_{CM} (denoted in the text by T_{CM}) vs center separation for four collisions of ^{86}Kr on ^{179}Au (E_{LAB} = 600 MeV, ℓ_i = 220 ħ; E_{LAB} = 800 MeV, ℓ_i = 220 ħ; E_{LAB} = 1000 MeV, ℓ_i = 220 ħ and 280 ħ.) The time evolution of the collisions is indicated by dots giving the position at intervals of 10^{-22} sec and the labels on the dots refer to the current orbital angular momentum. The upper part of the curve for E_{LAB} = 1000 MeV has two sets of dots, one for the trajectory starting with ℓ_i = 220 ħ and the other with ℓ_i = 280 ħ. (The trajectories are almost identical at first.) Note that the approach of the orbital angular momentum to its asymptotic value is not quite monotonic. The lower curve is the interaction energy between the two nuclei.

Fig. 10 The excitation energy per classical particle vs the phase of oscillation of a spherical container with infinitely hard walls. The dimensions of the container and the initial distribution of particle velocities were chosen to approximate a nucleus with 184 particles and the oscillation frequency was $\omega = 0.19 \times 10^{22}$ sec^{-1}.

Results for quadrupole (n=2), hexadecapole (n=4) and n=6 oscillations are displayed, showing a convergence towards the wall formula prediction (solid line). The dashed line shows the result for a parallelepipedal box oscillating about the cubical shape, with the same rms amplitude as in the other cases.

Fig. 11 The same spherical container as in Fig. 10 is oscillating in the quadrupole mode with the same amplitude and frequency as before. The partly reversible bumpy structure in the excitation energy per particle, ascribed to the symmetry of the quadrupole mode, can be destroyed by randomizing the particles' motions by making them jump after a given distance of travel (indicated, in fermis, on the right of the curve in question). When the jumps are every 1 or 2 fm the excitation curve is close to the wall formula prediction.

Fig. 12 A comparison of the wall formula with classical and quantal computer studies. The oscillating container in the classical calculation is the same as in Fig. 10 and in the quantal calculation it is a Woods-Saxon potential well with a diffuseness parameter a = 0.66 or a = 0.1. The multipolarity of the oscillation is n = 4, the frequency in 1.08×10^{22} sec^{-1}, and the number of doubly filled orbits is 56 (N = 112).

Fig. 13 This is similar to Fig. 12 but the shape of the container (or Woods-Saxon well) is an exact spheroid, oscillating about a deformed prolate shape with a ratio of axes of c:a = 1.4305. The frequency is 1.52×10^{22} sec^{-1}.

Fig. 14 Same as Fig. 13 but the frequency is 0.76×10^{22} sec^{-1}.

Fig. 15 Same as Fig. 13 but the frequency is 0.38×10^{22} sec^{-1}.

Fig. 16 Same as Fig. 13 but the frequency is 0.19×10^{22} sec^{-1}.

Fig. 17 Comparison of the wall formula with a quantal calculation for the excitation energy in the case of particles in a well following a sequence of saddle-to-scission shapes. The quantal result is based on following 144 neutrons (i.e. 72 doubly occupied eigenfunctions) in the diffuse well shown in Fig. 18. The time development of these shapes is based on a classical hydrodynamic calculation including a viscosity of 0.02 terapoise, which results in the viscous damping shown by the dashed curve. The full circles give the quantal excitation energy with respect to the ground state of the system with the appropriate shape. The open circles are an estimate of the irreversible part of this excitation (see text). The dotted curve is an indication of how the one-body dissipation would be expected to deviate from the wall formula prediction in the vicinity of scission.

Fig. 18 The 10,30,50,70 and 90 percent contours are shown for three shapes in the saddle-to-scission sequence used in the calculation underlying Fig. 17.

Fig. 19 The boundary of the velocity distribution function in the immediate vicinity of an element of area moving normally with respect to a long mean-free-path Fermi (or Knudsen) gas, originally at rest and characterized by a limiting velocity v_F. The particles about to strike the surface are to the right of the dashed line, those that have rebounded are to the left. In (a) the element of

surface is moving towards the gas with a speed less than v_F, in (b) with a speed greater than v_F, and in (c) it is moving away from the gas with a speed less than v_F.

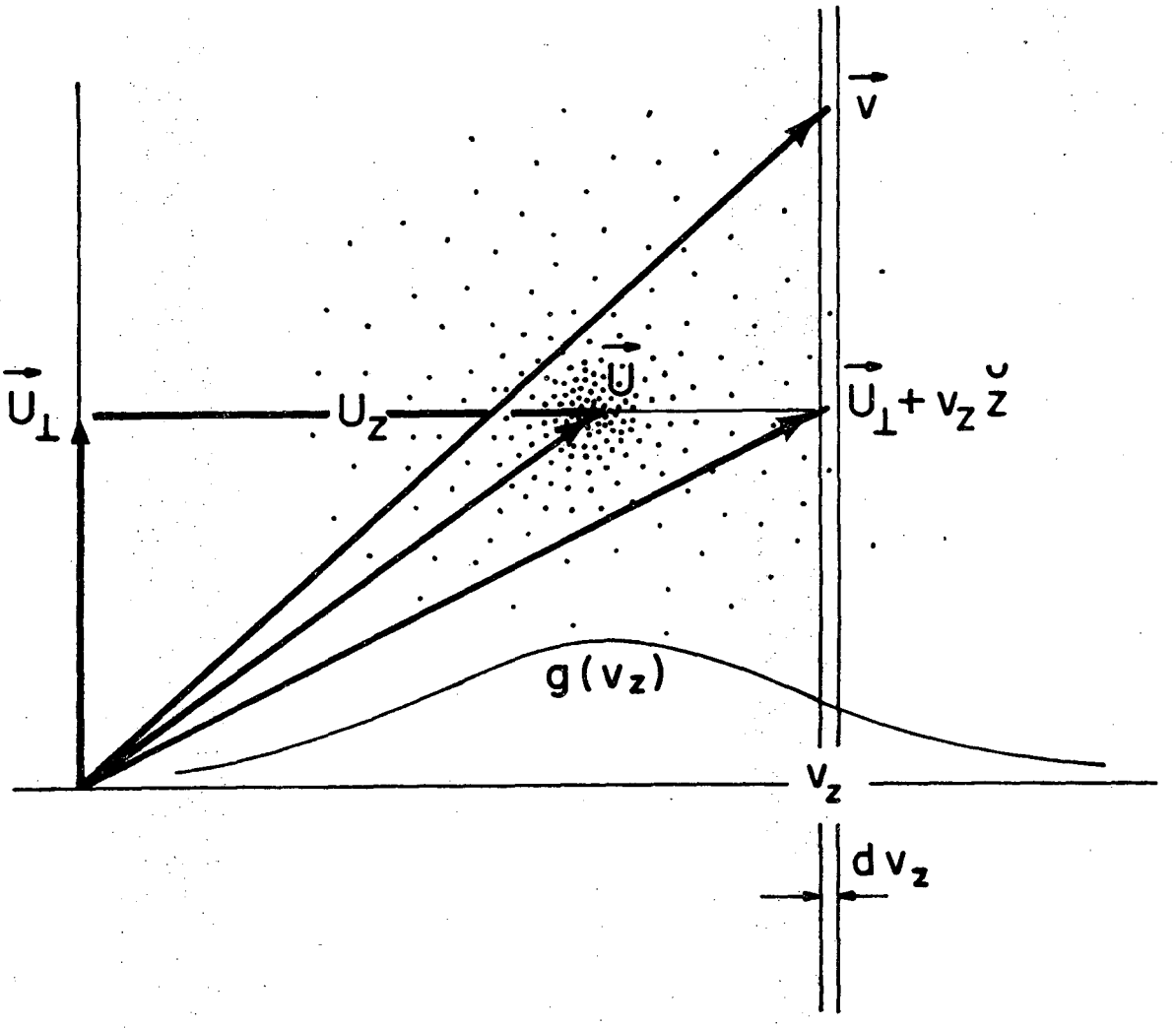

XBL776-1326

FIG. 1

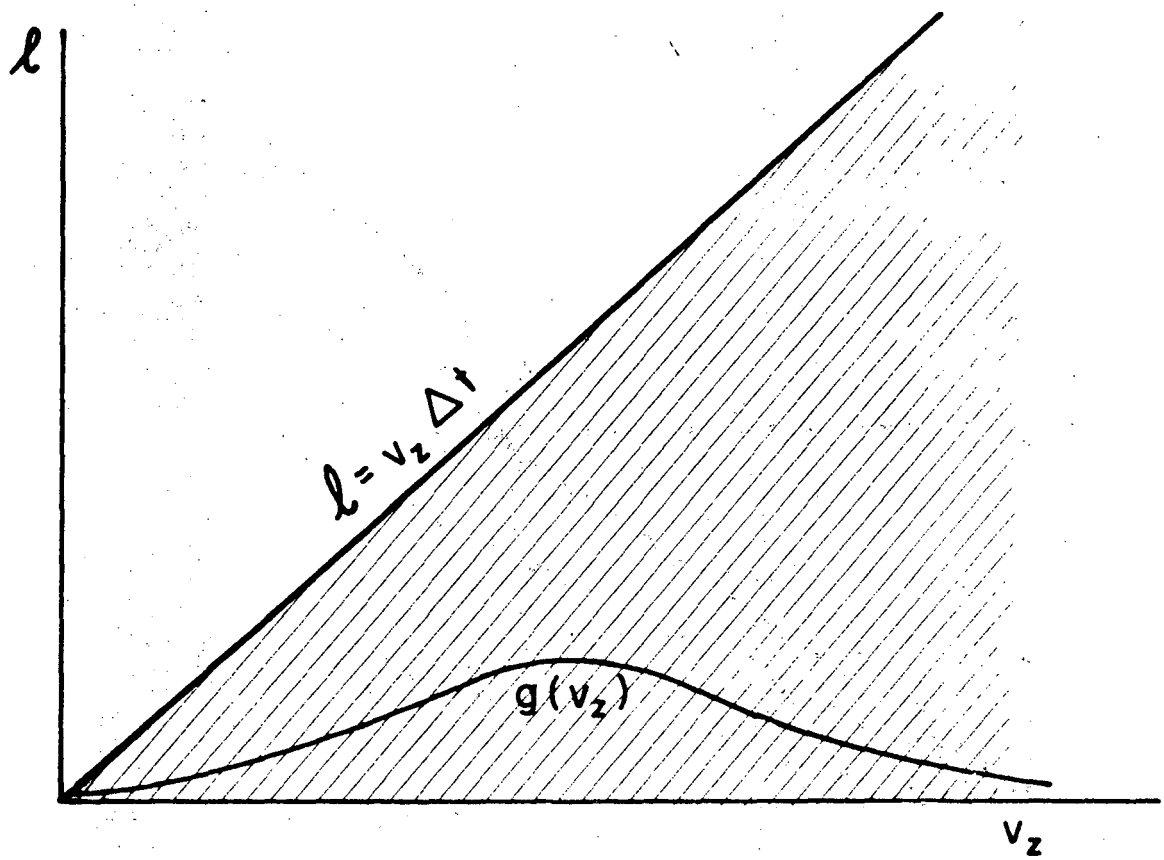

XBL776-1325

FIG. 2

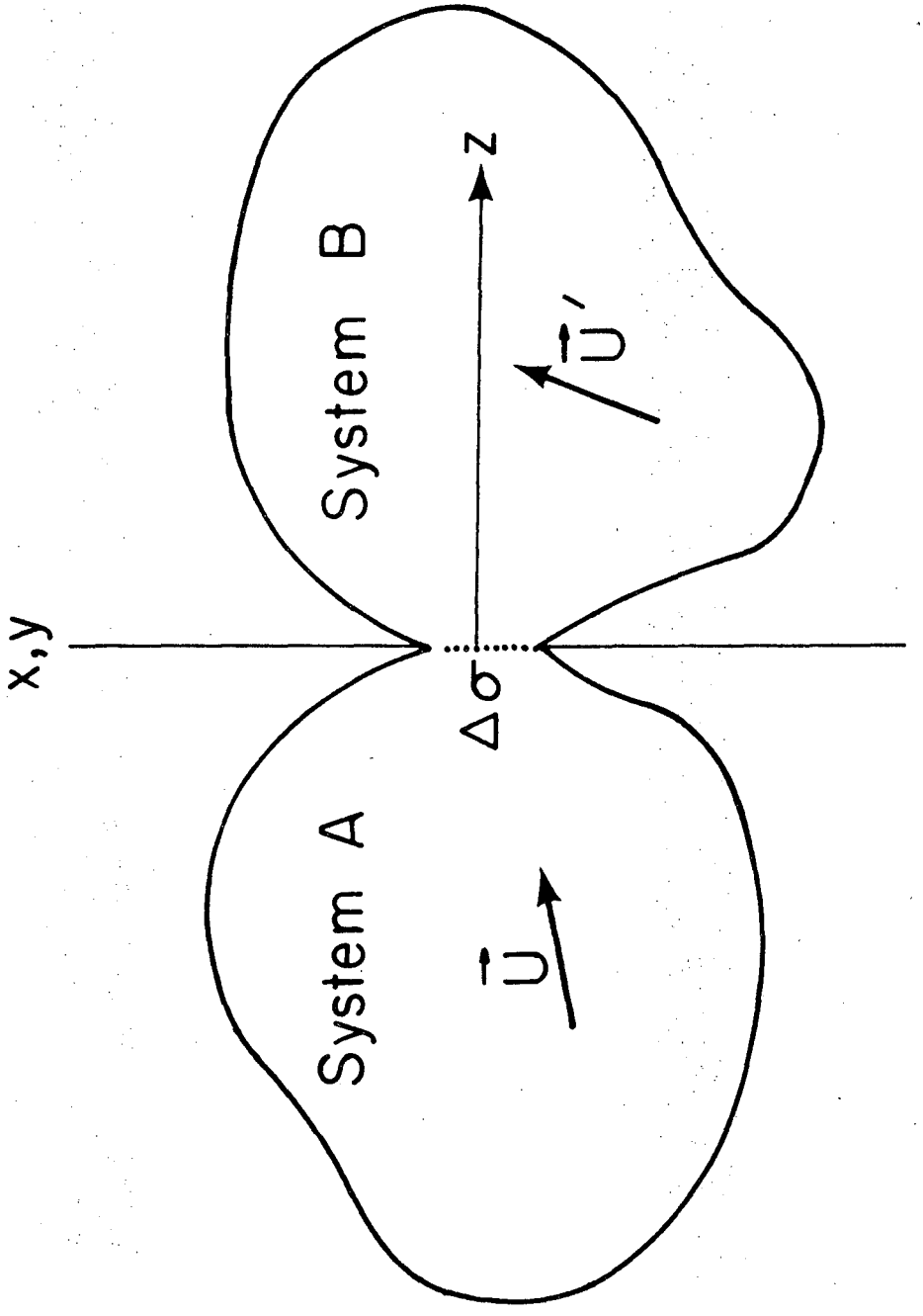

XBL776-1327

Fig. 3

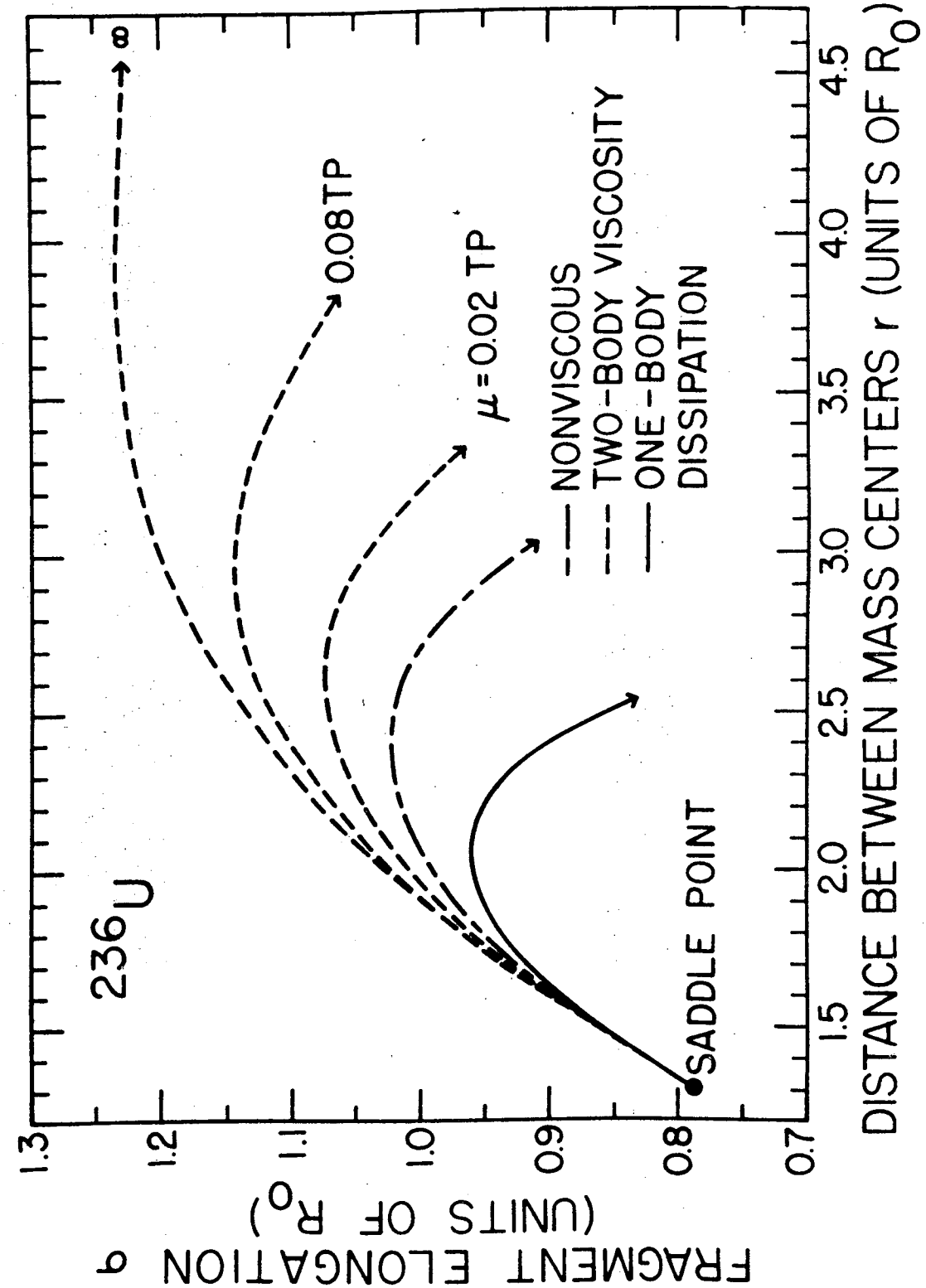

XBL 777-9490

FIG. 4

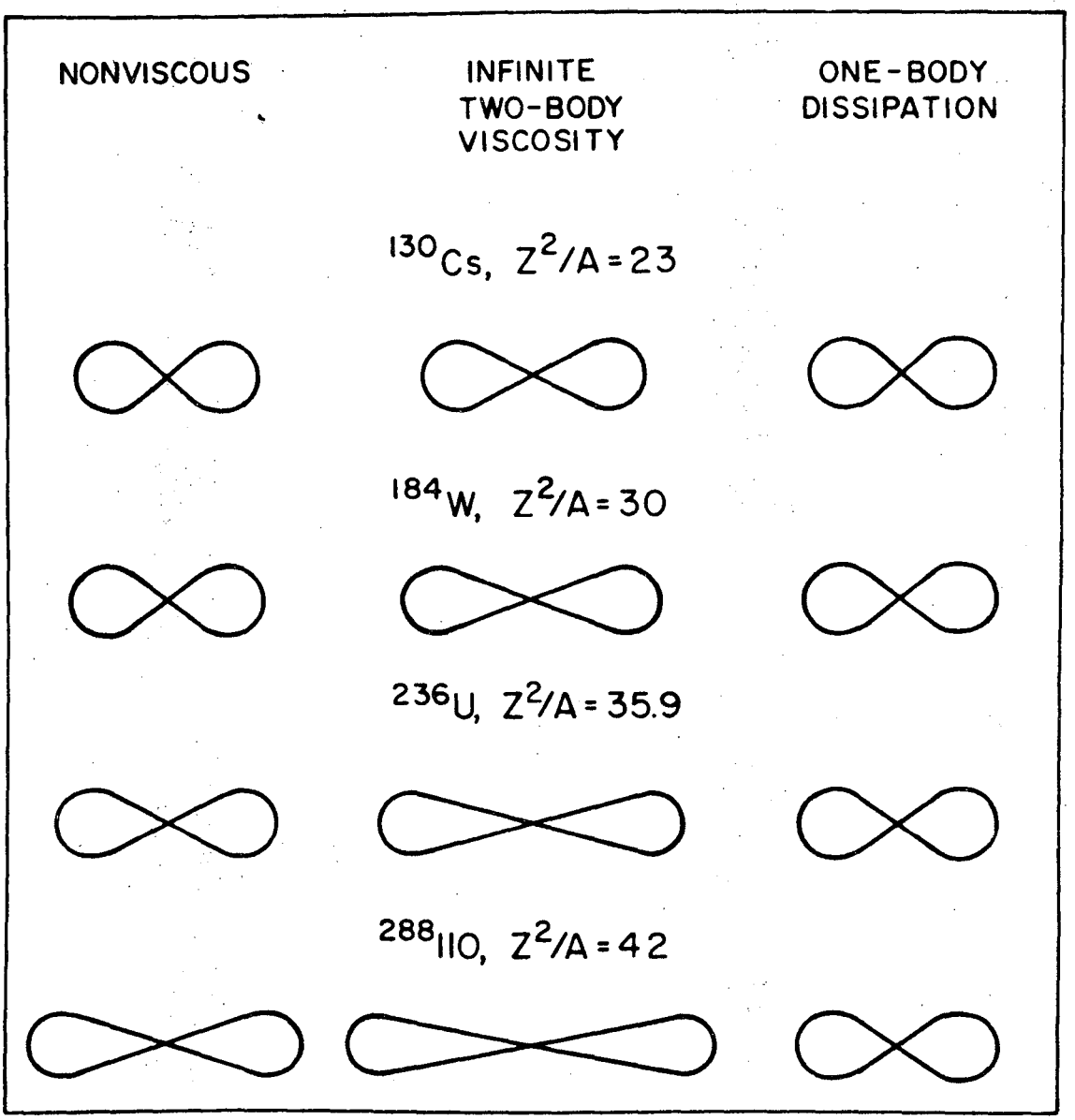

XBL 777-9491

FIG. 5

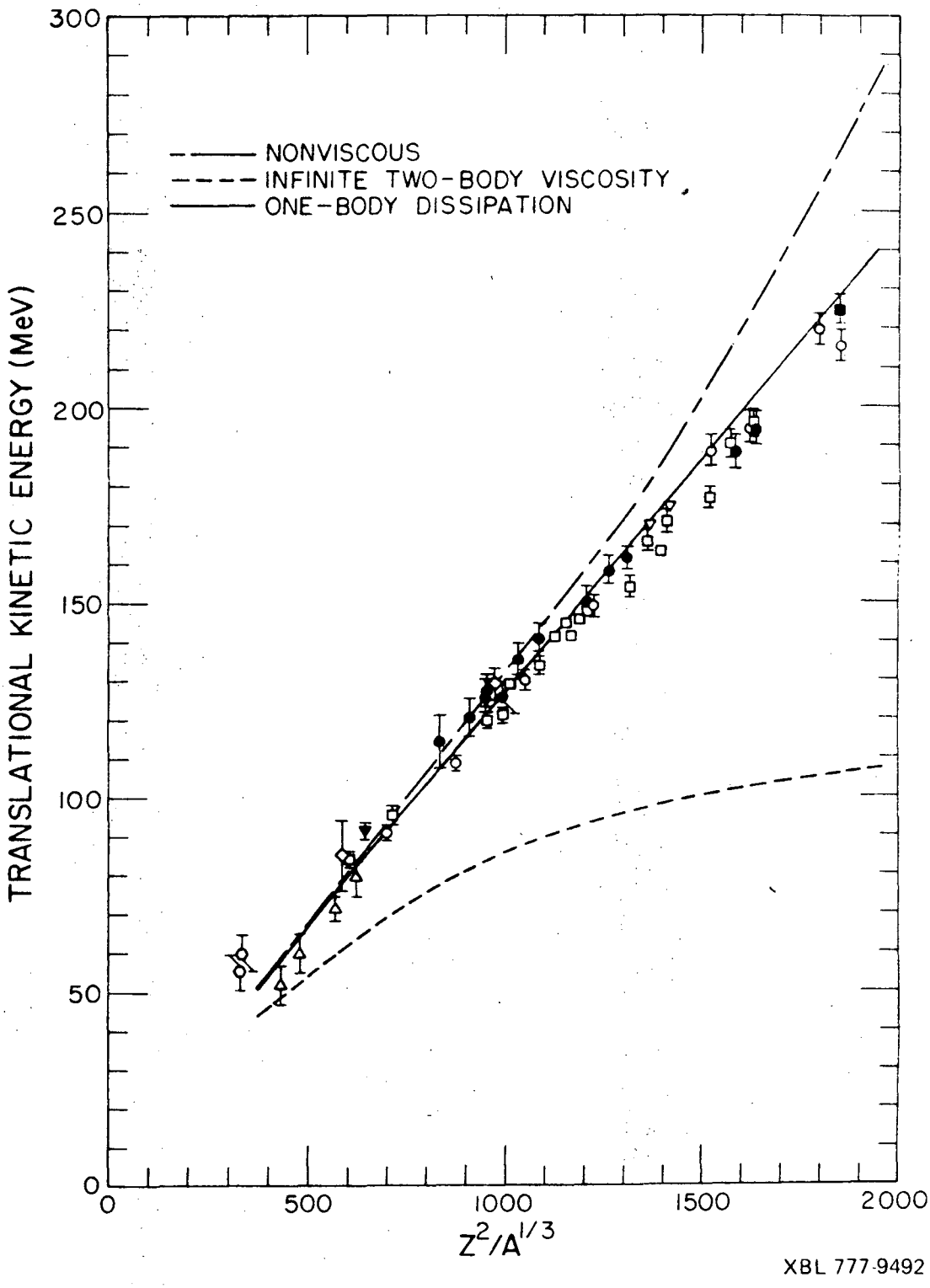
NONVISCOUS
INFINITE TWO-BODY VISCOSITY
ONE-BODY DISSIPATION
TRANSLATIONAL KINETIC ENERGY (MeV)
$Z^2/A^{1/3}$
0
50
100
150
200
250
300
500
1000
1500
2000
XBL 777-9492

FIG. 6

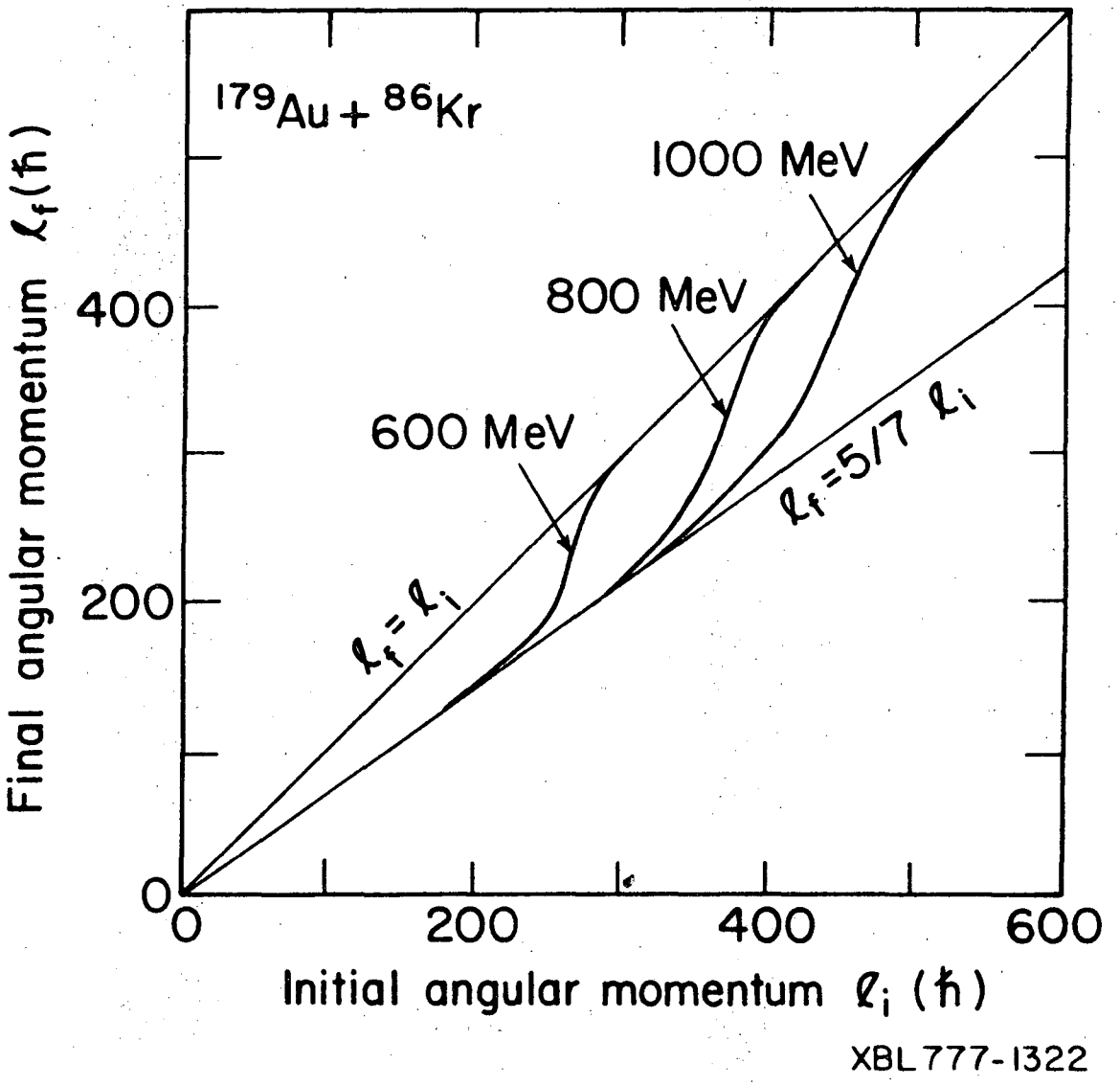

FIG. 7

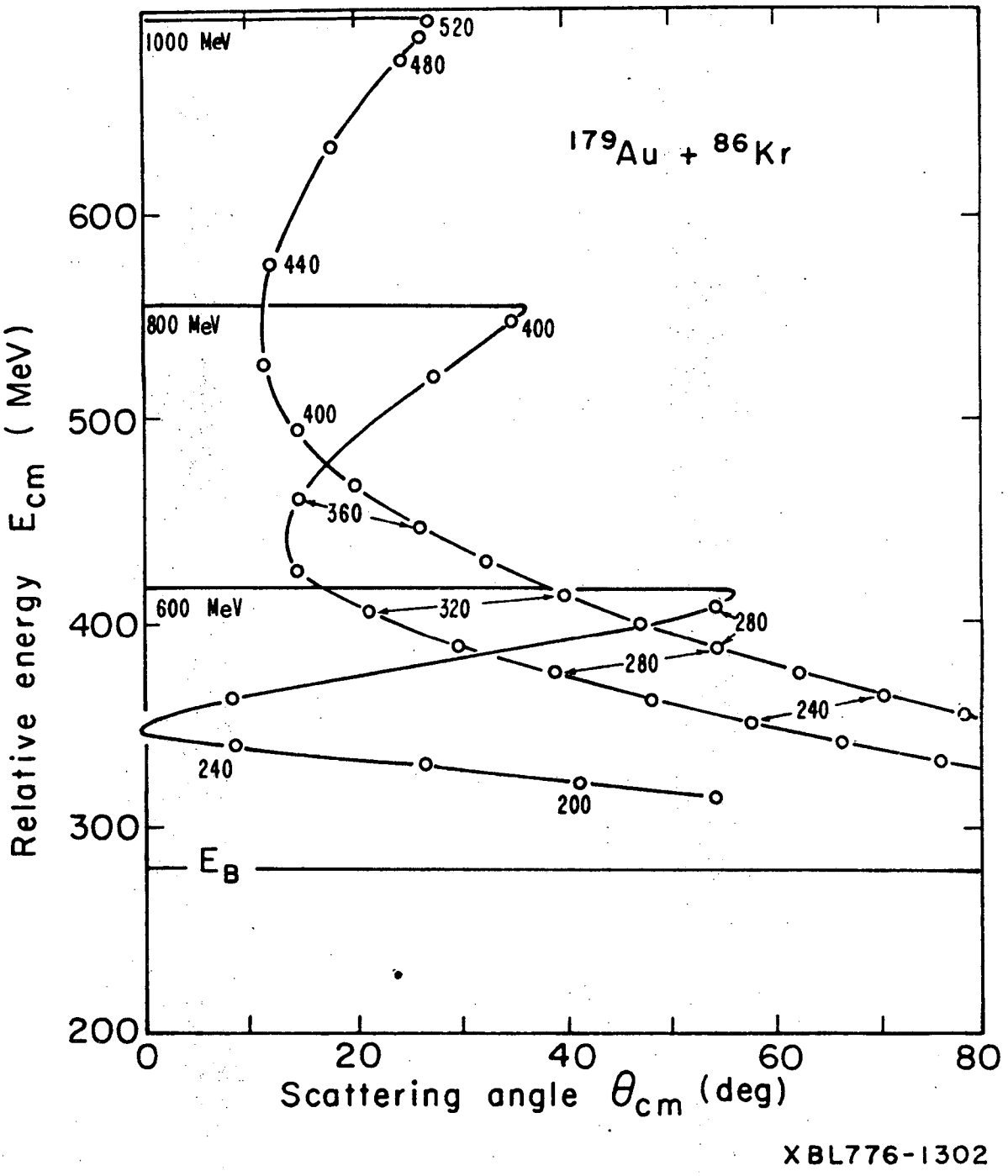
1000 MeV
520
480
$^{179}Au + ^{86}Kr$
600
440
800 MeV
400
400
500
360
600 MeV
320
280
280
400
240
240
200
300
E_B
200
0
20
40
60
80
Relative energy E_{cm} (MeV)
Scattering angle θ_{cm} (deg)
XBL776-1302

FIG. 8

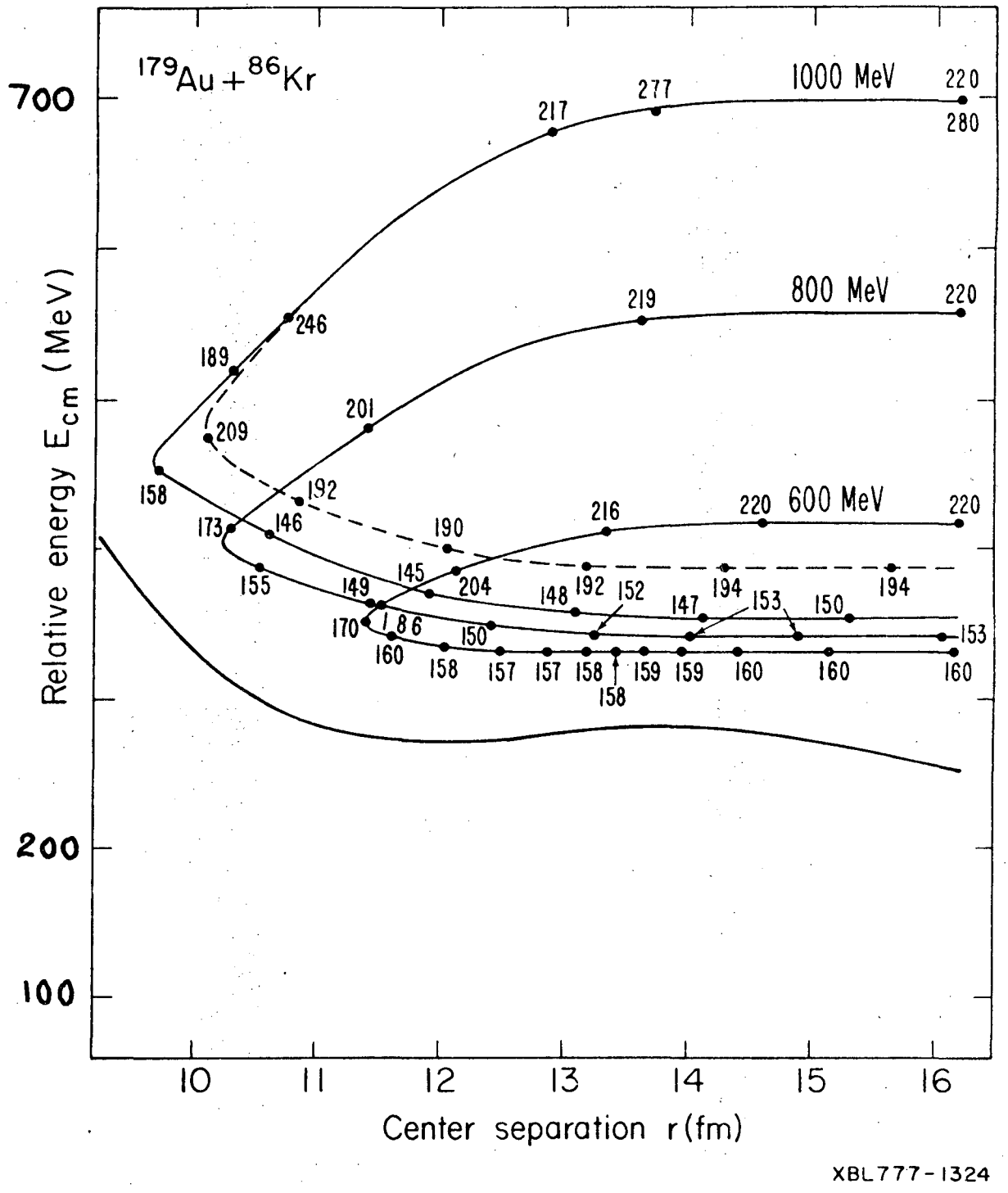

XBL777-1324

FIG. 9

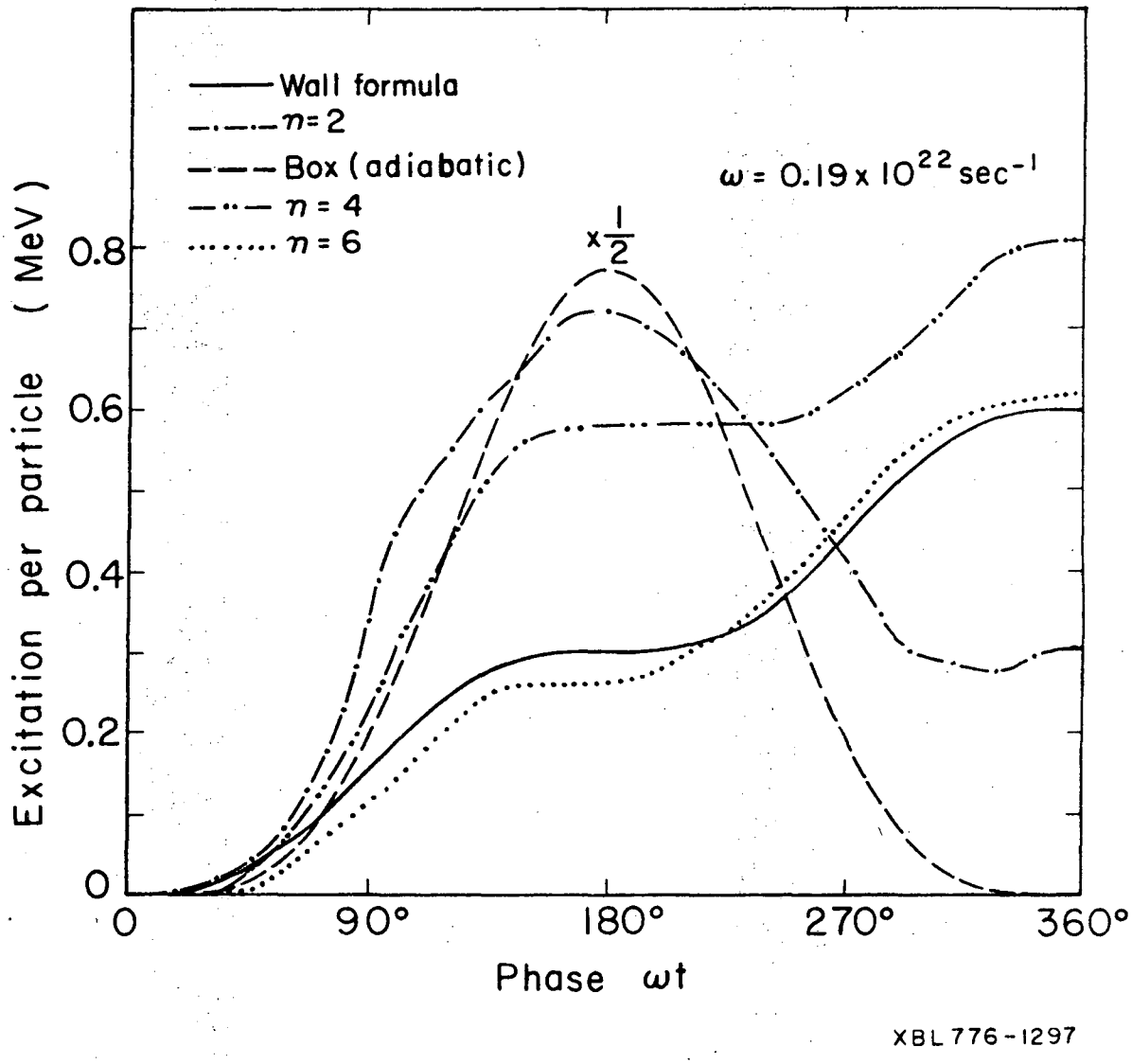
Wall formula
n=2
Box (adiabatic)
n = 4
n = 6
ω = 0.19 x 10^22 sec^-1
x 1/2
Excitation per particle (MeV)
0
0.2
0.4
0.6
0.8
0
90°
180°
270°
360°
Phase ωt
XBL 776-1297

FIG. 10

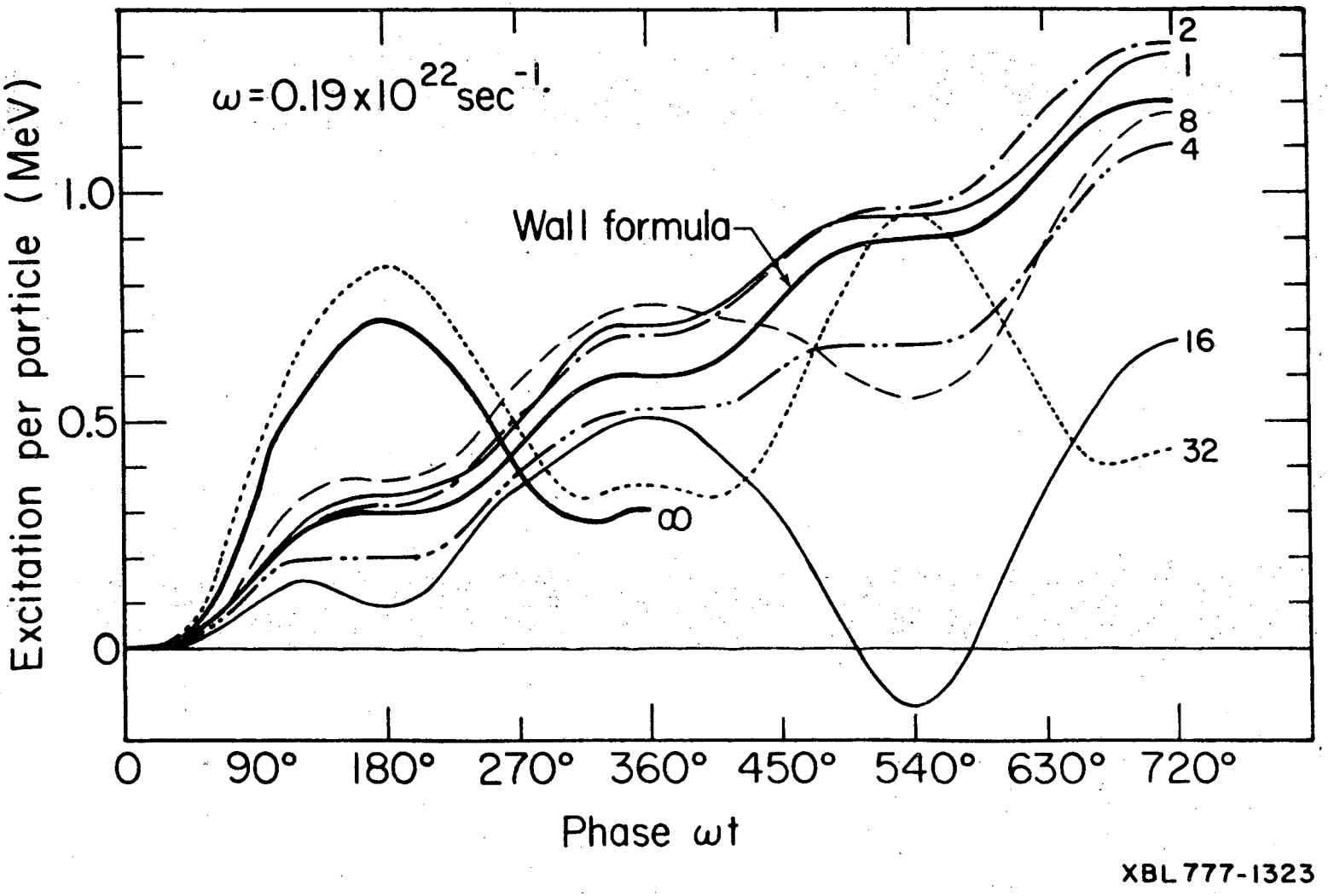

FIG. 11

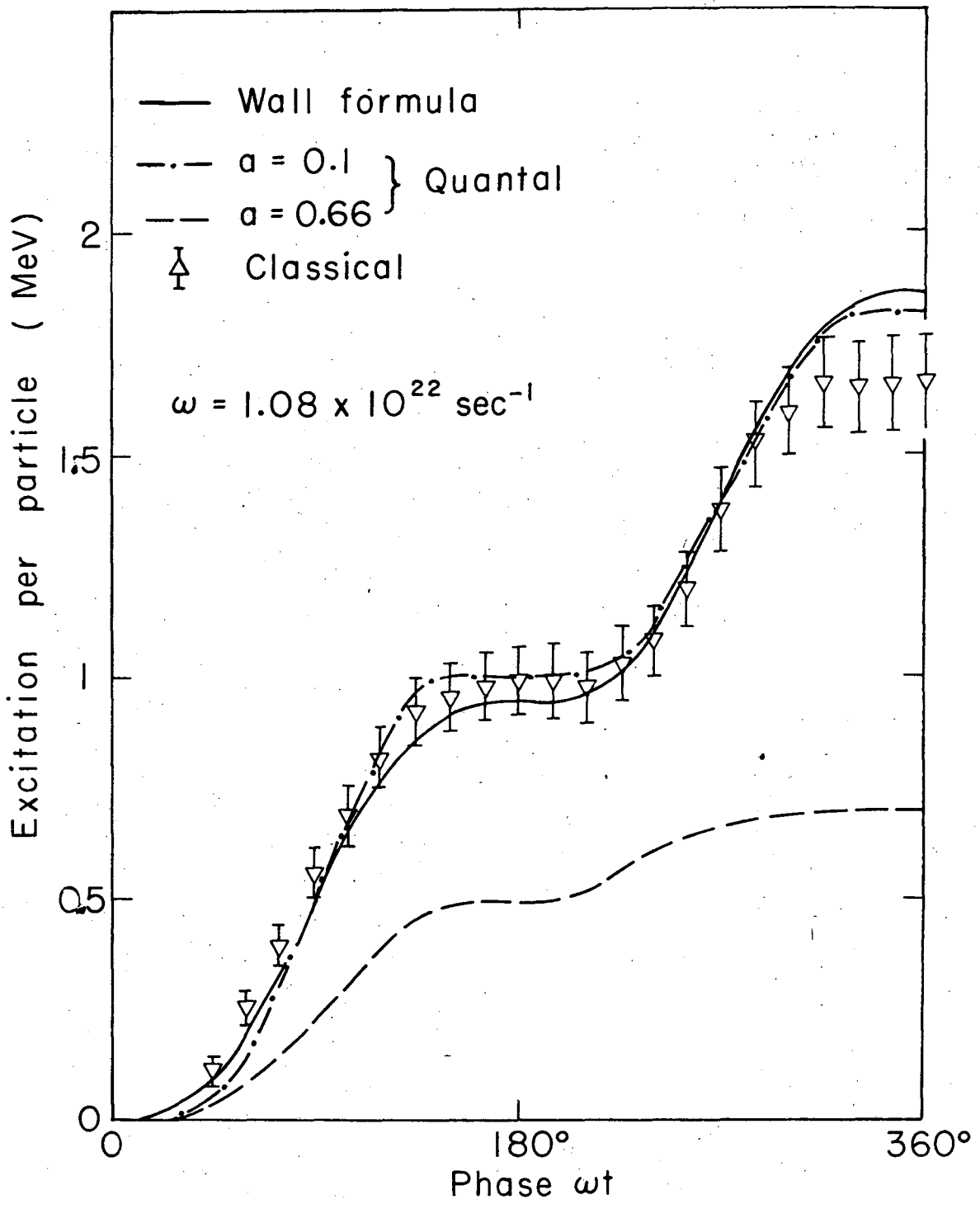

XBL776-1300

FIG. 12

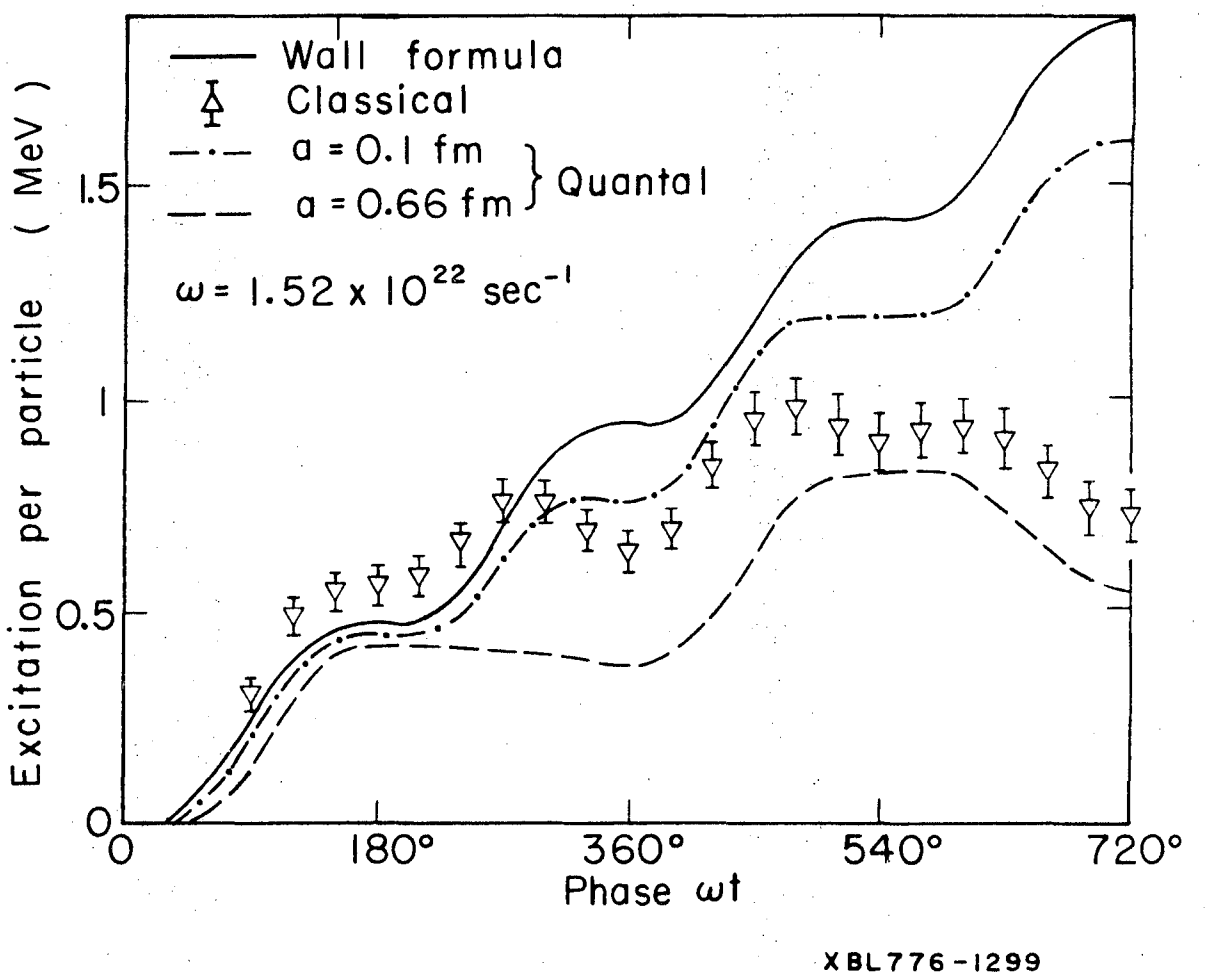

FIG. 13

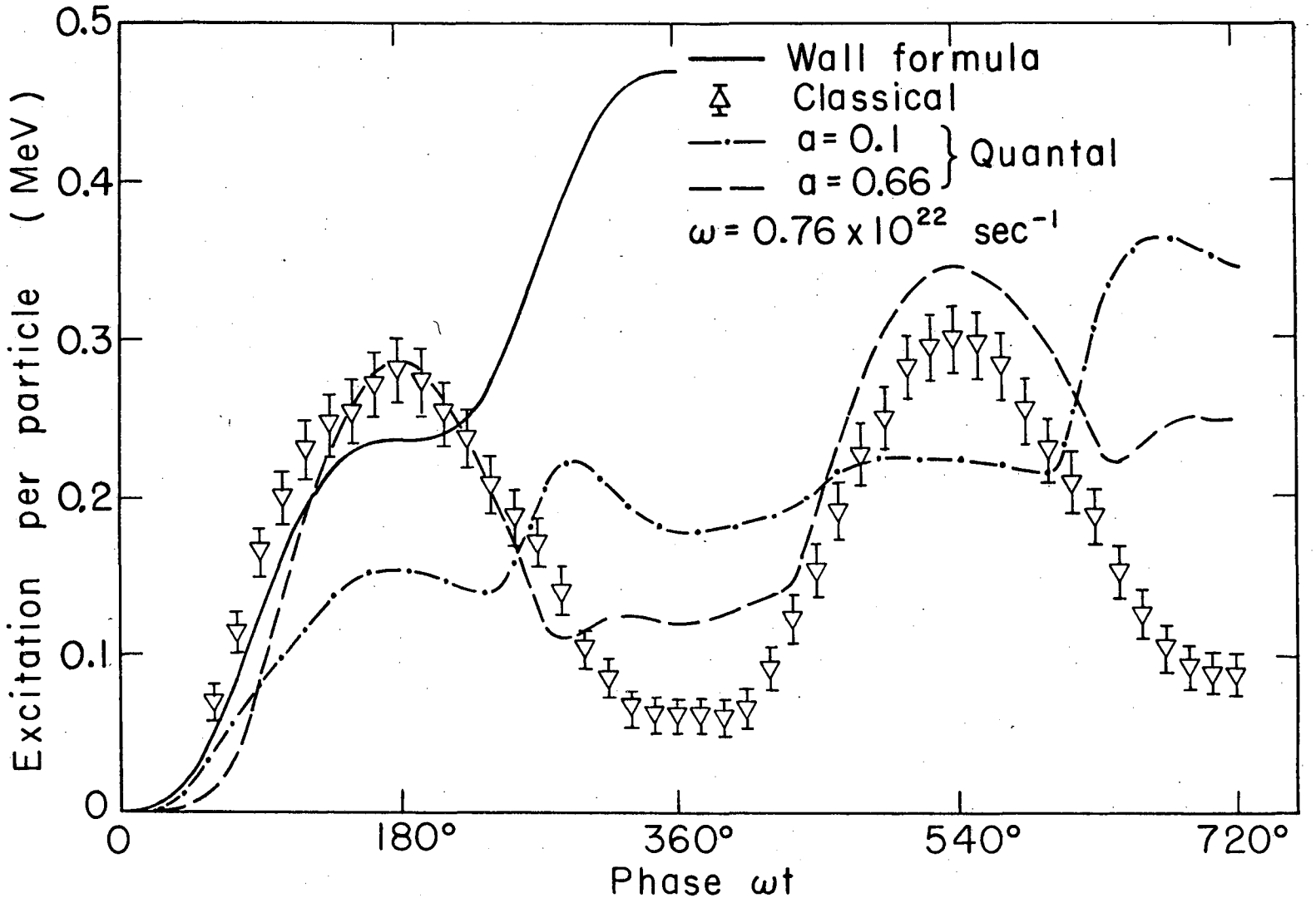

XBL776-1301

F16.14

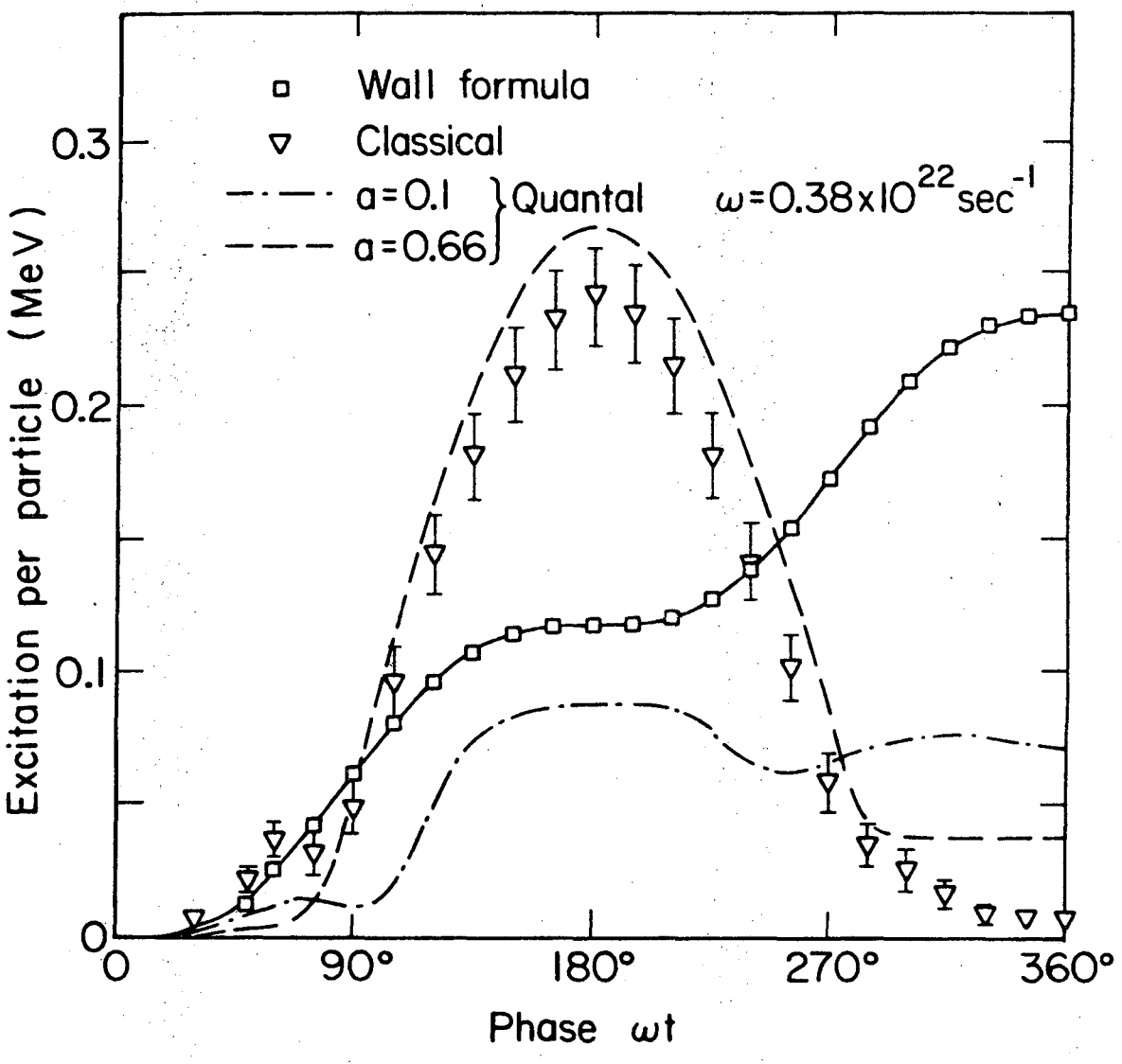

FIG.15

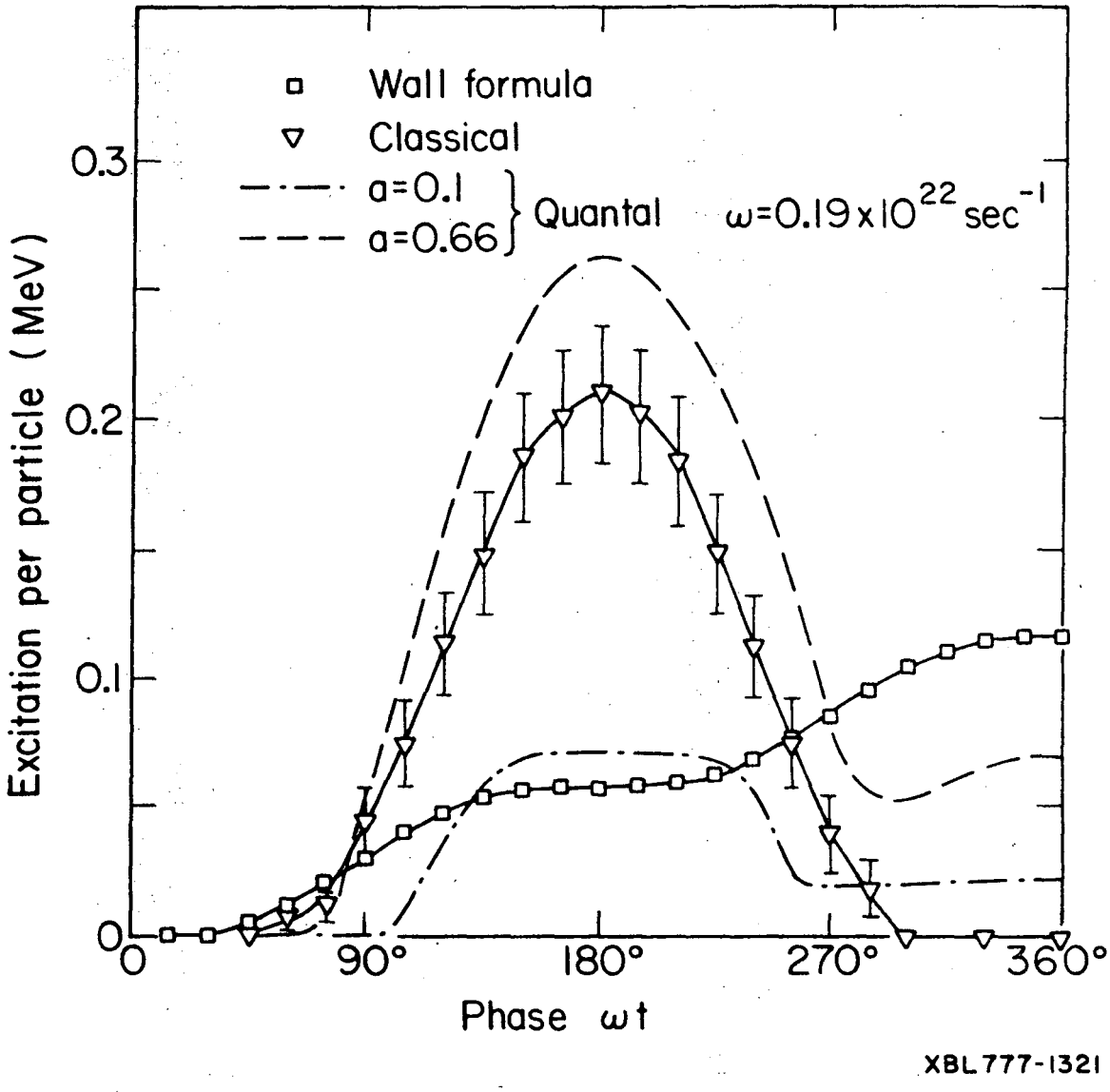
Wall formula
Classical
a=0.1
a=0.66
Quantal
ω=0.19x10^22 sec^-1
Excitation per particle (MeV)
0.3
0.2
0.1
0
0
90°
180°
270°
360°
Phase ωt
XBL777-1321

FIG.16

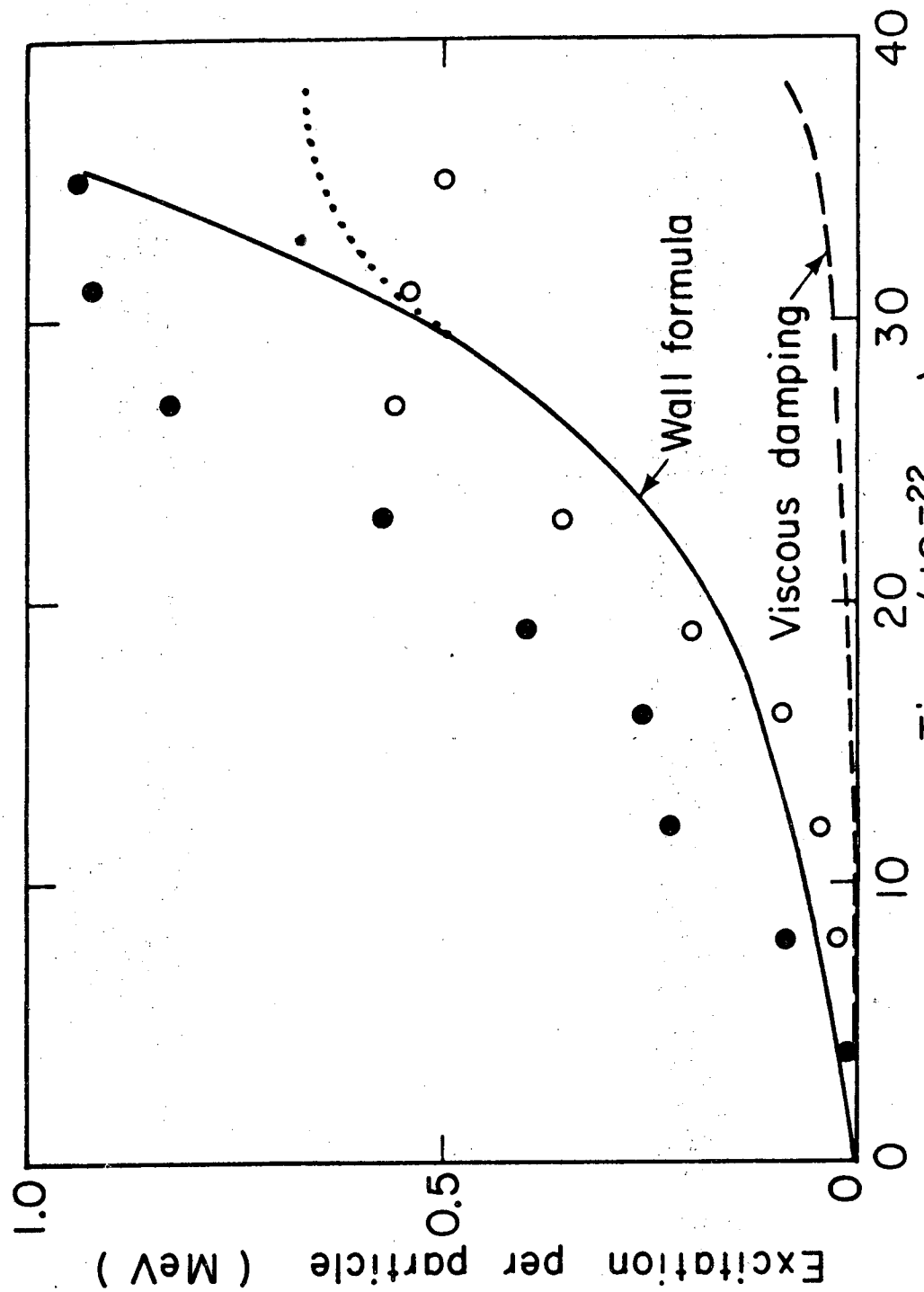

XBL776-1298

FIG.17

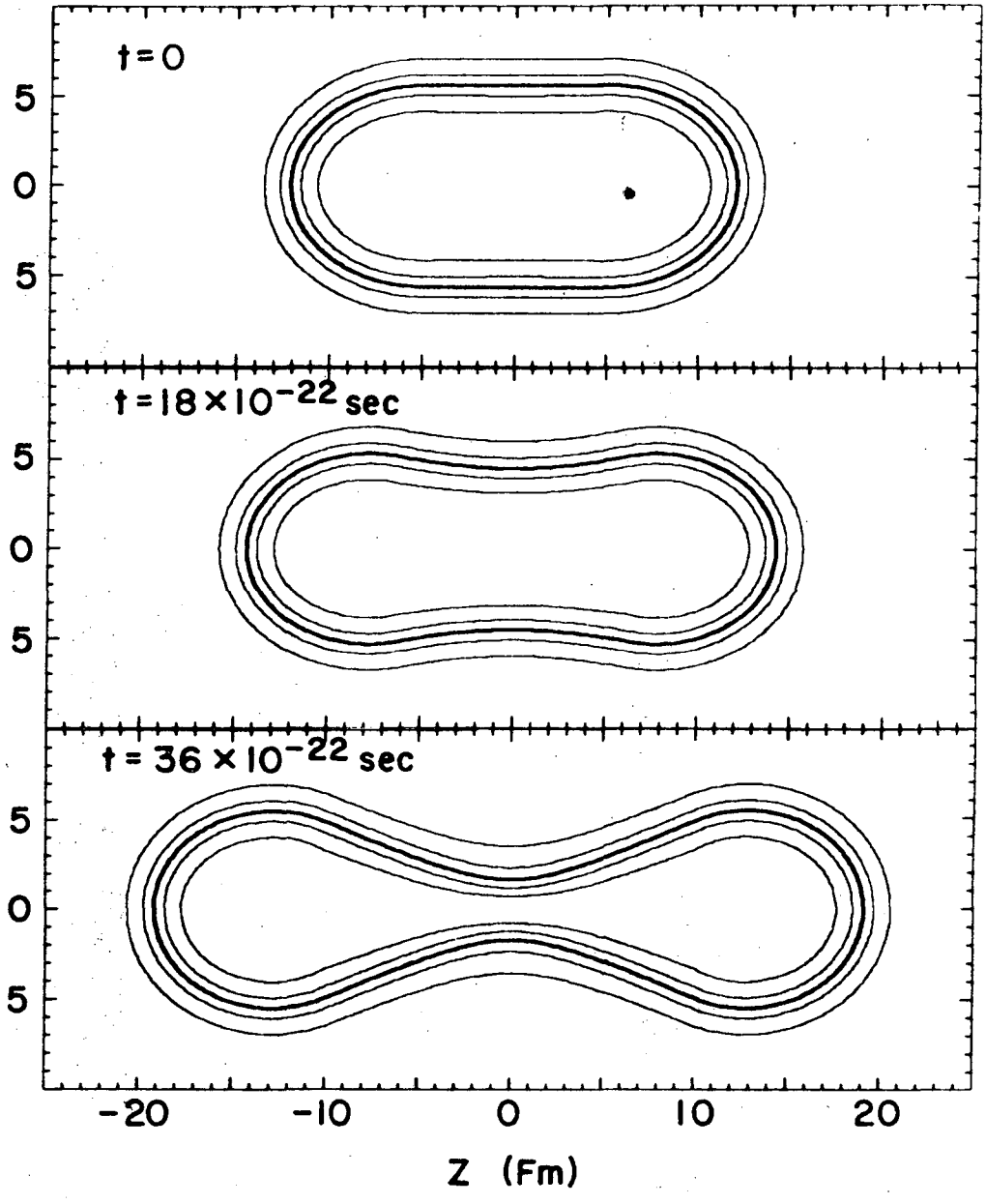

FIG. 18

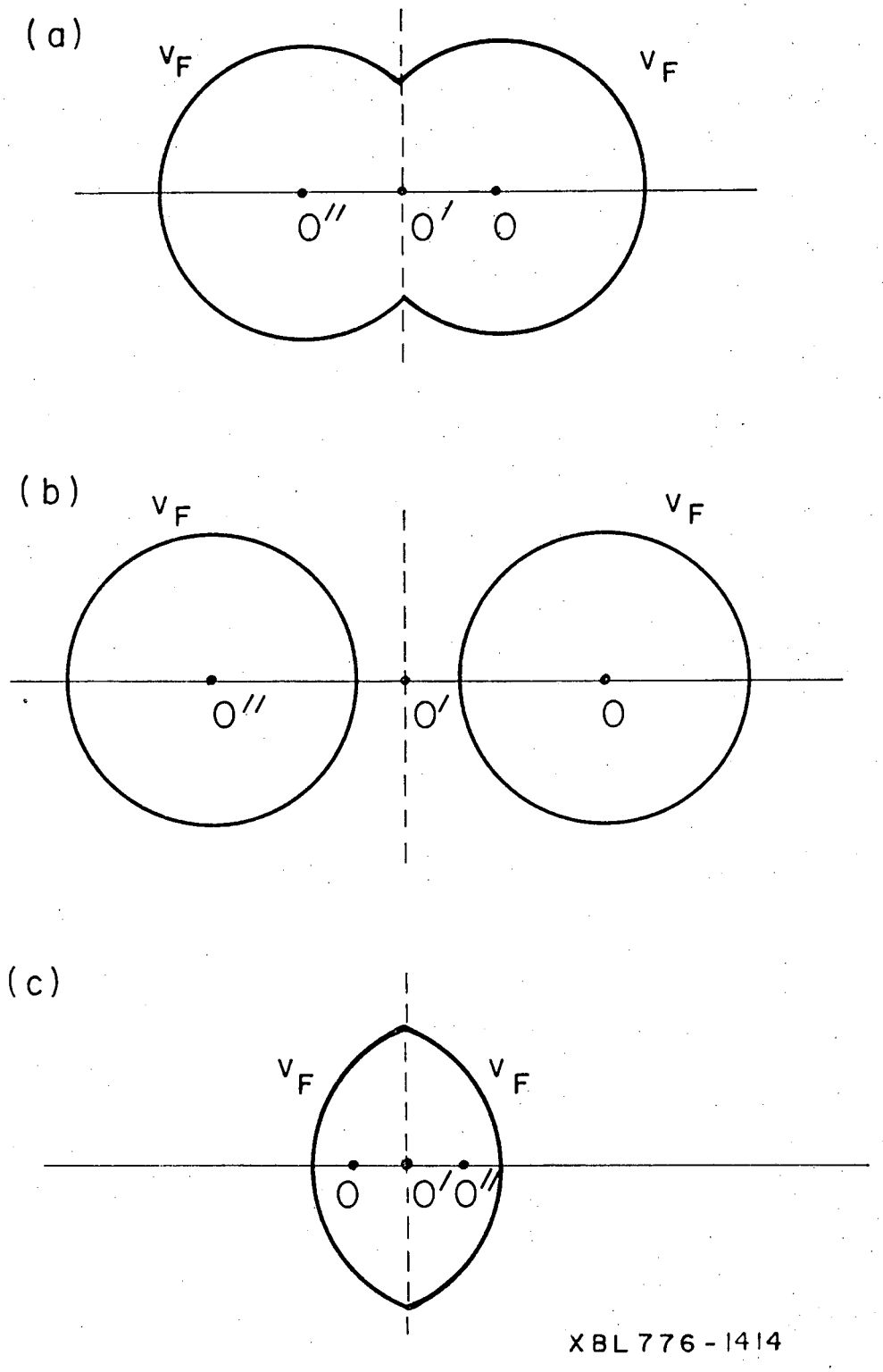

FIG. 19

TECHNICAL INFORMATION DEPARTMENT
LAWRENCE BERKELEY LABORATORY
UNIVERSITY OF CALIFORNIA
BERKELEY, CALIFORNIA 94720